Delft University of Technology
Master of Science Thesis in Embedded Systems

A reliable modulation scheme for body coupled communication with galvanic coupling

Mart Haarman

TU Delft Delft University of Technology

A reliable modulation scheme for body coupled communication with galvanic coupling

Master of Science Thesis in Embedded Systems

Networked Systems Group
Faculty of Electrical Engineering, Mathematics and Computer Science
Delft University of Technology
Van Mourik Broekmanweg 6, 2628 XE Delft, The Netherlands

Mart Haarman

9th of January, 2024

Author
Mart Haarman (m.b.a.haarman@student.tudelft.nl)
(tudelft-mart@haarman.info)
Title
A reliable modulation scheme for body coupled communication with galvanic coupling
MSc Presentation Date
The 18th of January, 2024

Graduation Committee
Dr. RangaRao Venkatesha Prasad
Dr. Qing Wang
Dr. Sujay Narayana

Abstract

This thesis explores the integration of (Frequency Shift) Chirp Spread Spectrum Modulation (FSCSSM) in Body Coupled Communication (BCC) using the Galvanic Coupling (GC) method. The goal is to provide a method of private communication in a noisy channel for devices in and around the human body. Various parameters, including frequency, electrode dimensions, electrode inter-distances, and noise levels, are evaluated. Results demonstrate that FSCSSM allows reliable communication in highly noisy channels, achieving a data rate of 9.6 kbps at a Signal-to-Noise Ratio (SNR) of -9dB. The impact of body composition is highlighted, showing its significance in single-body communication. The communication in single-body is extended by evaluating body-to-body communication, enabled by touch, as well. This research provides valuable insights for designing robust BCC-FSCSSM systems.

Preface

In our daily lives, we often gravitate towards the latest technologies and gadgets, embracing the newest trends without fully considering how these "things" communicate and exchange information. Many users lack the knowledge or motivation to understand the extent of privacy risks associated with using new digital consumer applications. As someone who values privacy, I believe that the engineering community should play a role in safeguarding the privacy of their product's users.

Body Coupled Communication, a field of research dating back to at least 1996 (which happens to be my birth year), initially focused on private communication. However, upon further exploration, I discovered that over the years, the emphasis on body communication has often prioritized data rate rather than privacy. This led me to take a step back and contemplate the possibility of developing a novel method for reliable and private body-coupled communication. In my view, establishing a strong foundation will ultimately enable the creation of a system with data speeds tailored to specific applications, rather than the other way around.

When I contemplate the potential of body-coupled communication, my imagination runs wild with possibilities. By confining signals within the body, we not only enhance privacy in communication but also alleviate congestion in free-space bandwidth. In crowded areas, for instance, playing music through Bluetooth headphones can lead to interference when many individuals are using Bluetooth-based wearables like smartwatches and headphones. These wearables typically do not require high data rates, and they consistently make contact with the human body, making them ideal candidates for body-coupled communication. Being able to contribute to technologies that benefit human beings and have the potential to reach a wide range of users is something that truly excites me.

Drawing inspiration from the concept behind LoRa, I aim to apply my skills as a student of Electrical Engineering and Embedded Systems. This project will involve delving into Chirp-Spread-Spectrum communication methods, designing hardware, and programming embedded devices, all to explore and implement body-coupled communication.

My general interest lies within engineering, not research. For that reason, I looked up to doing a master's thesis because of the vast amount of research that has to be performed. But, in the end, I'm grateful that my supervisors gave me this opportunity and handed me a topic which I found very interesting after all. I would like to thank, Dr. Sujay Narayana and Dr. RangaRao Venkatesha Prasad, for taking the time with me, sitting down with me to find this very suitable and challenging topic and helping me to accomplish my work. A special thanks to Dr. Sujay Narayana for being in contact with me daily and guiding me through this process.

Also, during work, I had a lot of help from fellow students for gathering data. I would like to thank them for their patience, time and help. Lastly, I could not close off this section without thanking my friends and family for supporting me over the last period in which I worked on this thesis.

Mart Haarman

Delft, The Netherlands
20th January 2024

List of abbreviations

A
ADC Analogue to Digital Converter
AFE Analogue Front End

B
BCC Body Coupled Communication
BER Bit Error Rate

C
CC Capacitive Coupling
CSV Comma Separated Values

D
DAC Digital to Analogue Converter
DFT Discrete Fourier Transform
DSSS Direct-Sequence Spread Spectrum

E
e.c. Equivalent Circuit
EM Electromagnetic
EO electro-optic
EQS Electro-Quasi-Static

F
FDA U.S. Food and Drug Administration
FEC Forward Error Correction
FEM Finite Element Method
FDTD Finite Difference Time Domain
FFT Fast Fourier Transform
FIFO First-in-First-out
FM Frequency Modulation
FPGA Field Programmable Gate Array
FSCSSM (Frequency Shift) Chirp Spread Spectrum Modulation
FSK Frequency Shift Keying
FT Fourier Transform

G
GC Galvanic Coupling

H
HPF High-Pass Filter
HBC Human Body Communication

I
IFFT Inverse Fast Fourier Transform
IoT Internet of Things

K
kbps kilo-bit-per-second

L
LPF Low-Pass Filter

M
Mbps Mega-bit-per-second
MC Magnetic Coupling
MoM Method of Moments

O
OOK On Off Keying
op-amp Operational Amplifier

P
PAN Personal Area Network
PER Packet Error Rate

R
RF Radio Frequency
Rx Receiver

S
SDR Software-Defined-Radio
SF Spreading Factor
SNR Signal-to-Noise Ratio
SPI Serial Peripheral Interface

T
Tx Transmitter

V
VHDL Very-high-speed Hardware Description Language

W
WBAN Wireless Body Area Network

Contents

Chapter 1

Introduction

By the day, the number of devices with the need for communication with one another increases. Part of these devices focus on applications in and around our bodies. With the growth of the number of devices and the Internet of Things (IoT), the necessity for private communication is not far behind. Just a few months ago it became known that Neuralink, a startup founded by the famous Elon Musk, has obtained approval from the U.S. Food and Drug Administration (FDA) to start clinical trials with brain implants[43]. These brain implants have the purpose of allowing the brain(human) to communicate with computers. At the time of their publication, a team of neuroscientists in Swiss allowed a paralysed man to walk again using a wireless, digital bridge between brain implants and the muscles[36]. The implants in his head communicate wirelessly with a headset. These forms of communication between man-made devices should be reliable and secure since human safety is an important, involved factor. But also, this communication should be private since it could contain sensitive information and the communication should also not be interrupted by an occupied bandwidth. In this thesis, I'm trying to provide a secure and stable method for wireless communication between devices in and around the body using Body Coupled Communication (BCC). BCC has two important advantages. First, it is a more private form of communication than Radio Frequency (RF) by coupling the signal to the body and preventing signal leakage. Second, bandwidth gets occupied only in, and very near to, the human body, preventing the flooding of available bandwidth in free space. This thesis will propose a method for a very robust and reliable means of using BCC, which allows applications to use BCC in the future for every use.

1.1 Background

This thesis combines (Frequency Shift) Chirp Spread Spectrum Modulation (FSCSSM) with Body Coupled Communication (BCC) as a novel approach for private communication. A bit of background is provided here on both these topics to understand what BCC is, why it has a private characteristic and what FSCSSM does to make BCC reliable.

1.1.1 Body Coupled Communication

Data transfer between devices can happen wirelessly or using wires. Bluetooth and WiFi are the most commonly known forms of wireless communication. For wired communication, a landline or internet cable are commonly known examples. Wired communication is fairly secure and cannot be sniffed unless physically making a connection with the wire. Wireless communication, however, is all around us and an attacker can pick up any signal that devices around transmit or receive. Although these signals are often encrypted, they still contain information that can be of use and encryption can be broken.
Devices in and around the body that need communication with other devices can choose between wires and wireless but wires cause practical implications. For implants, for example, wireless is preferred such that they can be placed with minimal occupation of space and wires sticking out of a human body are not ideal and could even be dangerous (think of getting caught up by something). Because a human body is constantly moving, a cable could wear out or limit movement.
Wireless communication might sound like the perfect solution. A downside is that wireless communic-

ation is often power-hungry and uses bandwidth that other devices might also want to use. Moreover, the signal is radiating in all directions and does not form a direct link between the transmitting and receiving devices. The latter can be used to intercept a signal.
Body Coupled Communication (BCC) is a means of communication with aspects of both wired and wireless communication. No physical wires are used but the signal does not radiate out in free-space so it cannot be intercepted without physical touch. In BCC, a signal is coupled to the human body (or any subject) and all the receiving devices are touching the same body to receive the signal.

The idea of BCC was first found by Zimmerman in 1996 [60]. In his paper, he describes that two researchers formed the idea of transmitting data through the body. One research focused on finding a means to interconnect body-borne information appliances, while the other group looked into applying electric field sensing for position measurement. From the two works, it was concluded that the Electromagnetic (EM) field that propagates through the body can carry information, implying that data can be transmitted using this EM field.

In BCC, either an EM field, a current or both are propagating through the human body from the transmitter to the receiver. Using low frequencies and low transmission power, the signal does not leak into the free space. Frequencies range from about 20kHz to about 30MHz but, as will be seen later on, more ranges have been studied as well.

To fully grasp what is propagating through the human body, one needs to understand the concept of EM waves. These waves are a type of energy propagating through a medium (the human body in this case) in the form of electric and magnetic fields oscillating perpendicular to each other and to the direction they travel in. These waves do not need a physical material to propagate through, they can also move in a vacuum. Visible light, light which humans can see, is also based on EM waves with frequencies from 430 to 750 THz (terahertz). Ships can signal S.O.S. codes to each other using light, which is an example of communication using EM waves. Other (commonly known) examples that use EM waves are Bluetooth and WiFi which have a base frequency of 2.4GHz or 5GHz(WiFi only). Sound is an example sample of a wave that cannot travel through a vacuum. Sound cannot propagate through a vacuum since sound requires molecules to oscillate, leading to a small airwave.

While EM waves do not require a medium to propagate through, since it does also propagate in a vacuum, it doesn't mean that a medium cannot weaken an EM wave. The human body has multiple layers such as skin, muscle, fat and bones which all influence the strength of waves and they are affected differently per frequency. Movement of the body can also affect the gain in the body and in addition, the body can pick up external signals, forming a noisy channel. Mostly for that reason, Radio Frequency (RF) is often chosen for applications in and around the body that communicate wirelessly with each other.

A signal can be coupled to the human body in various ways. Two of them are Galvanic Coupling (GC) and Capacitive Coupling (CC). These methods both make a device touch the body with one or two electrodes, which are conductors through which electric current enters or leaves a system. In his work[60], Zimmerman proposed a personal area network by using CC as a coupling method. His prototype used a frequency of 330kHz. CC is a coupling method that uses one signal electrode which is touching the body, and another reference electrode which couples, through the air, with ground. The latter coupling forms a return path and requires a (large) reference point that all devices couple to. The coupling is like in a capacitor where two plates couple with a dielectric in between. GC is a method in which two electrodes touch the body and an electric field arises between the two electrodes, forming a path for current to flow through the body. This method does not form a path through air to earth-ground, such as CC does and so, the signal is fully focused on the human body channel.

Main advantages of BCC are:

- **Limited occupation of bandwidth in free-space.** Since all the signal is coupled into the body, devices communicating on other bodies or outside of the human body are not interfered with by the signal.

- **Not interceptable without physical touch.** The signal is confined to the body and not radiated into the free space. Attackers cannot intercept the signal without physically touching the body. For this reason, the signal is private and more secure.
- **Power efficient.** The signal does not have to radiate into free space and transmission powers can be kept at a low level.
- **Does not require an antenna and hence can have a small package form.** The signal is coupled using (small) electrodes. For that reason, no antennas are required and the package can be kept small.

1.1.2 Galvanic Coupling

As mentioned, multiple methods can be used to couple a signal to the body. The most common methods are Galvanic Coupling (GC) and Capacitive Coupling (CC). This thesis has focused on Galvanic Coupling. The working of GC is briefly elaborated on in this section, more detail is provided in Chapter 3.

While CC was the first method to be introduced, Handa et al. introduced GC in 1997 [12]. An ECG signal was modulated into a very small current to be picked up by a receiver on the wrist. For both devices, they used two electrodes using only a power of $8\mu W$[12].

As was shown by Handa et al., Galvanic Coupling is a means of coupling a signal to the human body by making use of two electrodes[12]. An Electromagnetic (EM) field is created between the two electrodes by applying a potential difference between the two. This potential difference is modulated according to a modulation scheme which in this case is (Frequency Shift) Chirp Spread Spectrum Modulation (FSCSSM). The EM field propagates through the body channel, like in a waveguide, and forms a path for the current to flow. Receiving devices are provided with a potential difference across the electrodes caused by the EM field passing through them. A downside of GC is that much attenuation occurs and that has to be accounted for in the system. Moreover, there is a safety aspect since current is directly injected into the human body. The latter, however, should not be an issue when safety regulations are taken into account.

Main advantages of GC are:

- **Does not require a signal path outside of the human body.** The return path of the current comes directly from the reference electrode. No reference point is required as is in capacitive coupling. This allows operation at all places without compromise.
- **Privacy.** Since there is no air-coupling as is in CC, the signal is confined to the body and hard to intercept.
- **Reduced Sensitivity to Body Movement.** The relative electrode placement does not change when the body moves. In capacitive coupling the electrode reference coupling changes when the body moves. The stable signal is advantageous in scenarios where the body is mobile or moving a lot.

1.1.3 Frequency Shift Chirp Spread Spectrum Modulation

Frequency Shift Chirp Spread Spectrum Modulation or Chirp Spread Spectrum Modulation, FSCSSM and CSSM in short, is a method for modulating a signal to let the signal contain digital information.
In Body Coupled Communication (BCC), multiple methods can be used to store information such as simply switching on the signal for sending a digital one and switching off the signal for sending a digital 0. The latter method is called "On-Off-Keying". Most methods, however, either require much transmission power and/or are prone to interference. For applications in and around the body, such as implants, power efficiency is essential since implants often rely on energy harvesting or batteries that should last for a long period of time.

(Frequency Shift) Chirp Spread Spectrum Modulation (FSCSSM) is a modulation scheme that spreads

out digital information over both time and over a range of frequencies (bandwidth) but has a narrow cross-correlation peak in (matched) filters. The whole available bandwidth is used in this modulation technique. Using the whole bandwidth makes communication slow but reliable. The characteristics of FSCSSM make a modulated signal have a distinct waveform which leads to a very narrow but high peak when correlating the received chirp with the expected signal. This effect allows communication below the noise floor which is equal to an Signal-to-Noise Ratio (SNR) of 0dB. An SNR of 0dB effectively means that the average noise power is equal to the average signal power. Even when the average noise power is greater than the average signal power, this modulation technique allows for successful demodulation and retrieval of the intended digital data, up to a certain ratio.

The modulation of FSCSSM is a combination of, on the one side, transmitting a very narrow (short duration) but high-power pulse and, on the other side, transmitting a pure, single-frequency sine wave. A sine wave has an equal amplitude and a single frequency throughout the signal and lasts for a given period, allowing for low power transmission since the power is spread over time. Transmitting a high-power but very short pulse requires a lot of (instantaneous) power but the advantage is that its frequency spectrum is wide-band. A wide-band signal has the advantages of high capacity, noise resilience and high data rates.

The "chirp" in FSCSSM indicates that the waveform has a chirp characteristic in which there is not a single frequency but a sinusoidal-like waveform constantly increasing its frequency. The beginning of such a signal or chirp has lower frequencies with longer lasting periods compared to the frequencies at the end of the chirp. An example of such a chirp is provided in Fig. 1.1. The power is spread over the whole chirp by making the signal last for a while, like in a sine wave. By making the whole signal a sweep from one frequency to another over the whole bandwidth, the wide-band effect of a short high-power pulse is put into the signal. The details of how FSCSSM works, along with more visualisations is provided in Chapter 3.

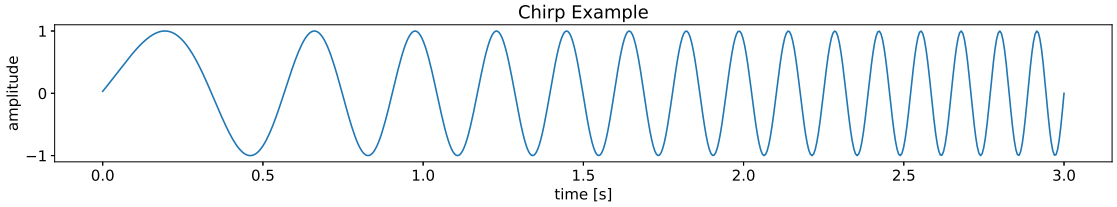

Figure 1.1: **Example of a chirp**

Radar systems make use of signal chirping since it requires little power, travels long distances and has a very narrow correlation peak when filtering. A narrow correlation strength provides for high distinguishability between objects that are located closely to each other. The power efficiency and long distances are achieved because of the chirping's robustness to interference as well as the efficient decoding possibilities. A reason for this modulation scheme being efficient is that it can be undersampled by the receiver and on those samples a single multiplication and Fourier Transform (FT) is sufficient to demodulate the chirp into a symbol.

A single chirp does not directly indicate that data is encoded into the signal. The chirp can be divided into smaller parts. By moving one part or more parts from the end of the chirp to the front of the chirp, data is encoded into the chirp. Essentially, this looks like a cyclic frequency shift and that's where the name ‗Frequency Shift Chirp Spread Spectrum Modulation comes from.

In FSCSSM each chirp has a symbol value meaning that each chirp can have a value between 0 and 2 to the power of the amount of bits in the symbol. A symbol is a given amount of bits forming one piece of data. The amount of bits in a symbol is determined by the Spreading Factor (SF). The SF tells in how many pieces each chirp is divided. The amount of pieces is equal to 2^{SF} and each of those pieces

is called a chip. Each chip lasts for a period of $\frac{1}{bandwidth}$. The bigger the spreading factor, the longer a whole chirp will last (lower data rate) but the more noise the signal can take.

Main advantages of FSCSSM are:

- **Power efficiency.** The signals require low power due to their characteristics and ease of (de-) modulation, allowing for low energy usage.
- **Robust to noise.** Because of the wide-band effect and high distinguishability of the signal modulated with FSCSSM, the signal can be demodulated even when the SNR is below the noise floor of 0dB.
- **Dynamism.** The scheme can be adapted by changing the centre frequency, bandwidth and the spreading factor. Each can be set accordingly for the channel that the chirp has to propagate through and the noise in that channel. All three factors pose a trade-off between data rate, resilience to noise and reliability.

1.1.4 Motivation

Nowadays, wireless communication is secured using the encryption of data that is being transmitted through the air, from device to device. The privacy of the communication is as good as the encryption of data in which often the metadata, that is attached to the packet information, is not encrypted. Besides, the more devices communicate in a given area, the more crowded the available bandwidth becomes and interference is more likely to occur. Confining the signal to the very near vicinity of and within the human body is an ideal method for making the signal resilient to leaking and interception. In a desired situation, all human bodies would have their wearables communicating by confining their signals to the near vicinity of the human body. In such a situation, these devices would not interact or interfere with devices on another body, so the available bandwidth would not flood. This is where Body Coupled Communication (BCC) comes in. BCC is a method of communicating in which the (human) body becomes the medium for the signal that carries information, to propagate through. This means that communication happens between devices that are in or on the body. Think of medical applications such as implants or entertainment applications such as earbuds or smartwatches.

Research on BCC has been going on since 1996 when it was introduced in a paper by Zimmerman[60]. Yet, only very limited real-life applications are in use that make use of it. Models have been proposed and a lot of aspects have been looked into and yet the main reason seems reliability issues. Medical applications could have the main benefits of a system using BCC because of its low profile and high level of security but such a system should, as expected, be very reliable. For that reason, this thesis will evaluate resistivity to noise. (Frequency Shift) Chirp Spread Spectrum Modulation (FSCSSM) could offer the reliability that BCC needs and that devices in and around the body need to communicate and the evaluations are used to show that.

T.G. Zimmerman proposed his Personal Area Network (PAN) [60] in the context of secure communication. In his proposal, the method used for coupling the signal to the human body was called Capacitive Coupling (CC). Studies on new concepts have been published throughout the years after 1996. These other methods contain Galvanic Coupling (GC)[4], Magnetic Coupling (MC)[32] and a combination of GC and CC. Those works improved data rate and tried to achieve a more stable channel for a communication method called BCC which is part of a more global scope named Wireless Body Area Network (WBAN), but robustness to noise was barely addressed.

Combining BCC with FSCSSM could offer a low-power, more robust and privacy-targeted method for communication. The main purpose of this thesis is to provide a proof of concept in which FSCSSM is used as a modulation scheme and validate its reliability concerning noise. Such proof of concept might form a baseline for further research and development of systems using the technology suggested in this thesis. Since the applications of BCC are not only limited to medical applications but also include social applications, this thesis provides insight into extending the body channel to other bodies by means of

touch. Such extension is called "inter-body communication".
Using GC as a coupling method contributes to the privacy aspect by not having to rely on a return path coupling through the air and helps by providing a stable path for the signal to flow through.

1.2 Problem statement

In Zimmerman's proposal[60], the method used for coupling the signal to the human body was Capacitive Coupling (CC). Studies on new concepts have been published throughout the years after 1996. These other methods contain Galvanic Coupling (GC)[4], Magnetic Coupling (MC)[32] and a combination of GC and CC. The works up to now mainly focus on data rate for which the highest data rates are achieved using CC. By looking at data rate, approaches proposed so far tend to move away from one of the aspects that make Body Coupled Communication (BCC) so powerful: secure and private communication. A more private method for coupling the signal is GC but this method also suffers more from attenuation in an already noisy channel.

In short, a system is needed to overcome a highly noisy channel using low frequencies while taking into account the main reason for this system which is enabling a secure and private communications system.

1.3 Research questions

Given the former problem statement and desire of the system outcome, a research question to be asked and answered in this thesis is **How does (Frequency Shift) Chirp-Spread-Spectrum Modulation contribute to the performance improvement of Body Coupled Communication with the use of the Galvanic Coupling method, while keeping in mind the original intention of body coupled communication?** To answer the main research question, some supporting questions have to be answered as well. The proposed additional research questions are listed here.

- What parameters define the reliability of Body Coupled Communication (BCC) and what should their values be?
- What are the limitations in which the BCC is a secure communication method?
- How does (Frequency Shift) Chirp Spread Spectrum Modulation (FSCSSM) improve reliability in comparison with research proposals from related or comparable works?

1.4 Scope and limitations

This thesis is meant to evaluate whether (Frequency Shift) Chirp Spread Spectrum Modulation (FSCSSM) is a good modulation scheme for Body Coupled Communication (BCC) and helps to set reliable communication in a body channel. While numerous aspects could be evaluated, the evaluation system is mainly designed and evaluated for the intended purpose which is to show that, with FSCSSM, BCC can achieve communication below the noise floor. This system will not be designed to compete with other works in terms of data rates although they will be evaluated. Signal leakage and radiation is not evaluated with this prototype but related works are used as a reference for signal leakage and radiation outside of the body channel. To show the effect of applying FSCSSM, frequencies achievable with available hardware are used and not the frequencies most desired for BCC because that might require other hardware.

In this thesis, Signal-to-Noise Ratio (SNR) will be evaluated for distance and body composition, centre frequency and bandwidth, distance between the electrodes, in- and output gain and both single-body- and body-to-body communication, solely using Galvanic Coupling (GC) as coupling method.

1.5 Challenges

The summary of work to present is an evaluation of Body Coupled Communication (BCC) with (Frequency Shift) Chirp Spread Spectrum Modulation (FSCSSM) as a modulation scheme using Galvanic Coupling (GC). Combining these three methods, of which BCC and FSCSSM were not related until now, poses some challenges.

The first challenge is hardware. A microcontroller will most likely not be able to sample at a high rate (microsecond order) and perform operations after each sample. Dedicated hardware is not around for this task so a workaround needs to be found using hardware that is available for the public.
An example could be using an Field Programmable Gate Array (FPGA). They still require a bit of knowledge and skill to program but do offer the resources to achieve this task. Another one could be using Software-Defined-Radio (SDR), which also requires a certain skill set.

When using GC as a means of coupling the signal to the human body, attenuation (especially at low frequencies) poses a challenge. The signal is weak and noise does easily add up to such a signal. The receiver should be able to filter, amplify and demodulate the received signal that has a weak signal strength.

Measurement errors pose another challenge. The body channels are different per day and even per hour. Temperature and body state change continuously and the body moves around. Measurements will have to be performed fully and not interrupted to be continued later, while some of them may take a while.

No implementation of FSCSSM has been found for BCC. That makes sense when this thesis proposes the combination as a novelty but does also mean that the whole implementation has to be completely custom-built. Building this system could be time-consuming and hard to debug.
The most commonly known implementation of FSCSSM itself, but not on BCC, is LoRa. Their hardware is closed source and the exact build of their packets is not published. Especially on how to synch with the preamble is not much detail available.

While research has shown many prototypes for a number of modulation schemes, only a few of them have their implementation published in detail. Compared to those works therefore is hard since building exact copies is hardly feasible.

1.6 Thesis outline

An outline of this thesis is provided herein which explains the structure of this thesis. In each section, the answers to the main research question and its sub-questions are gradually elaborated. Starting with this introduction where the general explanation of the system is provided along with the problem definitions and the research questions. Other useful related work is summarized, evaluated and accommodated with comments that compare to this thesis, in Chapter 2; Related Work. Using these related works, a theory of the proposed system combining (Frequency Shift) Chirp Spread Spectrum Modulation (FSCSSM) and Body Coupled Communication (BCC) is provided in Chapter 3; Theory. Using the theory and related work, a system model is composed. In Chapter 4 for both the transmitter, body channel and receiver a model is provided. For each model, the BCC and FSCSSM parts are discussed. These models describe how system components are designed for a prototype that can be used in evaluations. The outline of the model is understanding the components with relation to hardware and understanding the required steps to modulate and demodulate the digital data into an analogue signal and vice-versa. However, the Very-high-speed Hardware Description Language (VHDL) design on the Field Programmable Gate Array (FPGA)'s and software-based implementation is explained in Chapter 5; Frequency Shift Chirp Spread Spectrum in Body Coupled Communication. With the models and implementation that have been described up till Chapter 5, the whole system is evaluated and answers to the research questions can be provided. These evaluations and answers are incorporated in Chapter 6; Evaluation. Concluding remarks, discussion and conclusions are given in Chapter 7; Conclusions. Finally, Chapter 8 provides suggestions for future work based on the findings of this thesis. The Bibliography and Appendix are attached at the end of this thesis.

Chapter 2

Related work

The work presented in this thesis combines work put into and research on Body Coupled Communication (BCC) (or Human Body Communication (HBC)) and theory on (Frequency Shift) Chirp Spread Spectrum Modulation (FSCSSM) to improve stability in terms of symbol error rate. The goal is to keep the secure and private features of BCC intact.
Throughout the years since Zimmerman's work [60], sufficient amounts of research have been put into the broad variety of parameters involved in establishing an BCC channel. This section outlines that research and elaborates on choices made for this specific thesis, based on that research.
Specifically, related works are checked considering frequency, data rate & bandwidth, modelling & characterization of the human body channel, privacy, safety, the state-of-the-art work and finally FSCSSM.

2.1 Frequencies and data rate

The body has a capacitive, frequency-selective characteristic, meaning that no flat frequency response is present throughout the body. Besides the frequency selective characteristic, since every human body is slightly different, all human bodies have different frequency selective characteristics compared to each other as well. These different characteristics make a reliable and stable transmission of data harder to achieve because no single optimal frequency region exists for all bodies.

Often, the data rate is related to frequency with a higher frequency yielding a higher data rate. A high frequency is desired for fast data transmission but a too high frequency leads to signal leakage in Body Coupled Communication (BCC) which is a privacy concern. In this section, conclusions will be discussed regarding frequencies, data rate and signal attenuation. These comparisons will look into both intra- and inter-body communication and both galvanic- and capacitive coupling methods. Intra- and inter-body communication is also referred to as single-body- and body-to-body communication respectively.

An IEEE Standard has already been created regarding BCC. Part 15.6, 802.15.6 of the IEEE Standard for Local and Metropolitan Area Networks, suggests a centre frequency of 21 MHz for BCC. That, however, is not by definition the most desired frequency for BCC given the purpose for which BCC is applied. Moreover, the standard does not discuss the coupling method.

Multiple works provide insight into what frequency ranges could be applied to BCC. The main considerations of frequencies to be applicable to BCC are signal leakage, signal interference and gain(or attenuation). The most researched coupling method in BCC is Capacitive Coupling (CC). In 2014, Kiberet et al. performed research on the human body as an antenna concerning Human Body Communication (HBC) with CC as a coupling method. According to their research, provided in [19], the human body has a highly antenna-like effect in the regions of $50MHz$ and $80MHz$ due to its length. Moreover, Radio broadcast signals play a role from around $88 - 108MHz$, according to [5] which also researched with CC as a coupling method. Those broadcast signals can easily interfere with the human body channel. This interference is very likely because, due to the length of the human body or parts of it,

signals with these frequencies are picked up easily by the human body[5]. The reasoning for this is that the wavelengths of that frequency match double the length of the human body. Besides antenna effect and interference with other sources such as the Frequency Modulation (FM) band, higher frequencies tend to travel outside the body more easily than lower frequencies. In [56](CC), it is stated that $30MHz$ already poses too much signal leakage into free space. Das et al. did look into covert BCC and found that $23.88MHz$ was their theoretical limit for leakage-free BCC [6](CC). With those research findings taken into consideration, the $21MHz$ centre frequency suggested by IEEE 802.15.6 is on the safe side but close to the theoretical limit. As it turns out, most other works that will be mentioned below have chosen frequencies lower than $21MHz$. Besides, for Galvanic Coupling (GC) it was found that optimal frequencies are way lower, around 1 to 4MHz [22](GC) while most of the works mentioned above are using or looking into CC as coupling method.

Work	Year	Coupling method	Interbody	Frequency	Data rate	Bit Error Rate
[60]	1996	CC	no*	$400kHz$	$2.4kbps$	-
[42]	2004	CC	yes	-	$10mbps$	$4.7 * 10^{-8}$
[38]	2009	CC	no	$20MHz$	$10mbps$	-
[53]	2012	GC	no	$50kHz, 100kHz$	$5kbps$	-
[13]	2012	CC	no	$100kHz - 100MHz$	$10mbps$	10^{-3}
[50]	2014	GC	no	$125kHz$	$100kbps$	-
[34]	2015	CC	yes	$5MHz$	$200kbps$	10^{-3}
[44]	2016	GC	yes	$10.7MHz$	$57.6kbps$	-
[40]	2016	CC	yes	$100MHz$	$100mbps$	-
[23]	2017	CC	yes	$< 1MHz$	$130kbps$	$3.2 * 10^{-6}$
[48]	2018	CC	yes	$2 - 8MHz$	-	-
[27]	2018	GC	yes	$10.7MHz$	-	-
[17]	2019	GC	no	$100MHz$	$100mbps$	10^{-9}
[14]	2019	CC	yes	$20MHz$	$445kbps$	-
[7]	2019	GC	yes	$10.7MHz$	$9.6kbps$	-
[25]	2020	CC	no	$1MHz$	$8kbps$	-
[8]	2021	GC	yes	$10.7MHz$	-	-
[56]	2022	CC	yes	$415kHz$	$10's\ kbps$	-

Table 2.1: **Table with BCC prototypes and their results. GC = Galvanic Coupling, CC = Capacitive Coupling. *The paper by Zimmerman describes inter-body applications but does not provide an inter-body prototype.**

In Table 2.1, various works have been summarized that all have created a form of prototype to test their hypotheses. From this table, it can be observed that only two works ([13] & [17]) exceed the suggested limit of $23.88MHz$. With such a frequency, it is questionable whether this is true BCC or more profits from radiating signals.

A lot of research, among a few shown in Table 2.1, uses the $10.7MHz$ centre frequency. The reasoning for this is that these works are almost all established by the same research group and they have based their centre frequency use on another research group, active on the topic of BCC. They found 10 MHz to 50MHz to be one of the most optimal frequency regions to transmit signals through the human body [10] with. The reasoning for that is not specifically mentioned although most likely the components that they used dictated such frequencies. Other works from this research group are listed here:

1. [9] - Develops one of the first intra-body BCC prototypes using a $10.7MHz$ carrier frequency

achieving 9600 bps using Frequency Shift Keying (FSK).

2. [10] - Concludes that CC is superior to GC in terms of gain and high-speed communication.
3. [37] - As a novelty, an electro-optic (EO) sensor is developed as the receiver for BCC yielding a more sensitive receiver (7.3 times more sensitive).
4. [38] - A continuation to their 2004 research with the EO sensor provides an insight into the principles of BCC with an EO sensor. $10Mbps$ data communication is achieved.
5. [2] - Relations between transmitter electrode dimensions in GC and the received voltage are made in this work.
6. [39] - Evaluates the effect of the ground loop in CC in terms of signal strength.
7. [55] - Poses a study into the direction of electric field lines and direction of electric current in both GC and CC.
8. [27] - "A set of transmitter/receiver modules was designed to facilitate human body communication (BCC) between pairs of users." The prototype makes use of FSK at a $10.7MHz$ carrier frequency.
9. [30] - The work proposes an equivalent circuit model of the human body seen by the receiver to allow for a better Analogue Front End (AFE) design in the receiver for GC.
10. [28] - One of the group's first works of inter-body communication where they look into the signal propagation of BCC within two touching bodies.

In 2003, the group described the types of coupling that could occur among which GC as waveguide-coupling and CC as electrostatic-coupling [9]. In that work, they chose $10.7MHz$ as the frequency since the chips used in their prototypes are widely available for their use in FM-Radio [9](CC). A few of their works also look into and make use of, EO-sensors in the receiver, allowing for a higher sensitivity on the receiver side [37](CC) [38](CC) which was discarded in their later works for unknown reasons.

In Table 2.1, where prototypes have been listed, it is shown that most data rates are in the order of kilo-bit-per-second (kbps) to a few Mega-bit-per-second (Mbps). Only a few stand out obtaining Mbps orders, of which all of them have frequencies in the order of $100MHz$. Such frequency was earlier discarded as a valid and private use for body-coupled communication frequency. Another remark on the list is that research with higher data rates is using CC as the coupling method except for the work using the $100MHz$ centre frequency. By ignoring those works, it can be concluded that BCC is not about high-speed data communication but rather private and secure communication. From the table it is observed that two works achieve a 10 Mbps data rate, both of them use EO-sensors in the receiver. Both of them do not use a carrier wave but implement direct logic-high and logic-low voltages on the electrodes as ones and zeros. In [38](CC) the frequency is provided to be 20 MHz and due to their Manchester encoding, that yields a 10Mbps data rate. In [42](CC) a 10 MHz frequency is estimated since it was observed that they make use of On Off Keying (OOK) as an encoding scheme. Such schemes cannot be used below the noise floor and implementing techniques such as Direct-Sequence Spread Spectrum (DSSS) would either require a higher transmit frequency to obtain the same data rate or would, thus, yield a lower data rate for the same transmit frequency. The Signal-to-Noise Ratio (SNR) is not directly stated in either of these two works, but [42](CC) shows that they could achieve a 0.04% Packet Error Rate (PER) for intra-body communication and 3% PER for inter-body communication. For intra-body that corresponds to a $4.7 * 10^{-8}$ Bit Error Rate (BER) in their work[42].

A very detailed analysis of frequency regions in BCC was performed by Li et al. in 2017 [22], specifically for the body channel used with the GC method. They find that the best frequency region to use in GC is between 2 and 4 MHz for intra-body communication and between 1.5 and 2.1MHz for single-body communication, which complies with their theoretical models. For higher frequencies, the attenuation quickly becomes worse. While other works mention that higher frequencies might be optimal, these are either applied in CC or do not take into account that radiation starts to occur.

2.2 Modelling and characterization of the human body channel

To understand the behaviour of signals coupling to and propagating through the body, models and channel characteristics of the human body are required. Various works provide models and characteristics for both Galvanic Coupling (GC) and Capacitive Coupling (CC).

The models have been found for three different frequency regions. The first region is the frequency region up to 1 MHz ([3], [24], [1], [57], [26]). There is the frequency region between 1 MHz and 21 MHz ([19], [22], [30], [58]) which is most often referred to in literature for Body Coupled Communication (BCC) applications. Other publications describe characteristics for frequencies spanning both the two regions mentioned and/or higher frequencies.
Higher frequencies tend not to be interesting for BCC applications for privacy reasons [6] and, as is already mentioned in the previous section, they are not suited for GC due to their tend to radiate outside of the body.

A method used for modelling is Finite Element Method (FEM), in which the body is seen as a finite amount of small elements and the analysis of each small element combined is the analysis of the whole.
In [29], a FEM model is created of two (simplified) human bodies to simulate the effects of frequency, modulation scheme and termination in the sense of impedance, on (over the air) capacitive coupling between two bodies. The frequency in this model is swept from 100 kHz to 1 GHz. They look into the possibility of snooping and successfully decoding a signal. What they find is that, for CC, the possibility to attack a system is possible for the CC coupling method but highly depends on the strength of the signal at the transmitter. The attack is easily prevented by having a low signal strength, especially for lower frequencies ($< 1MHz$).
Over-the-air capacitive coupling is modelled, simulated and measured using FEM in [58] as well, for frequencies between 1 and 10 MHz, which is the near-field region. By doing so, the distance at which the signal can be snooped using another body can be simulated. The obtained model can simulate the channel characteristics for the near field (1-10 MHz, 0 - 1.5m) with a maximal error of 0.92 dB according to real measurements. Again, this research does not include the GC coupling method and they make no comments regarding privacy but the general finding is that lower frequencies have less channel gain and are, thus, less susceptible to attacks.
These FEM models confirm that the first frequency region is most optimal concerning privacy.

The research in [3] provides models for both GC and CC in the same paper. That work aims to find an application range for both techniques. For CC, distance was not considered to be a relevant issue up to 150 cm. The leakage however is deemed more relevant for these higher frequencies. A different frequency range is used for CC in this research. For GC the experiments were evaluated from 0 to 200kHz and for CC the frequencies evaluated range from 1 to 100MHz. For GC, this range was found to be 15 cm. In the publication, distances greater than 15 cm were not measured so attenuation of greater distances is not reported. In [1], distances up to 50 cm have been reported in models, only within the Electro-Quasi-Static (EQS) frequency region.
The EQS region contains frequencies 1MHz. For those frequencies, the electro-quasi-static approximation can be applied. By applying the electro-quasi-static approximation, Maxwell's equation can be simplified to the Laplace equation in their work. While not used in this thesis, this indicates that at lower frequencies, models can be simplified. In [22], a model is proposed which achieves inter-body communication through a handshake, up to 240 cm but the frequency region in their model is up to 6 MHz and so, according to some definitions, no longer in the EQS region and, thus, deemed less/not private. In that same model, the optimal frequency for inter-body communication was found between 2 and 4 MHz when using GC, while being between 1.5 and 2.1 MHz for BCC on a single body. As was mentioned in the previous section, they did verify their calculations using actual measurements which did fall in line with the calculations.

In Table 2.2, a list of literature is presented with publications that do model the channel that is used in their BCC research. It can be deduced that almost all works come up with some kind of Equivalent

Circuit (e.c.) model to characterize the human body channel. Not only the body is modelled as a channel, but also the air between two bodies. In [29] & [58], the effect of inter-body coupling without touch is modelled and compared with measurements, to look into private communication. These researches were previously mentioned in the FEM analysis works and their general finding is that lower frequencies have less radiation effect but both of the works are concluding based on analysis of CC.

Inter-body coupling with touch, which means a physical connection between two bodies, is modelled in [22] & [1]. These models take into account body composition (layers) such as bone, skin, muscle and fat and analyze the effect of those layers, the effect of distance and the effect of various frequencies. Both these proposals are providing models for GC. They conclude that lower frequencies have less attenuation, so higher frequencies are better in terms of signal propagation. However, the model in [22] states that, for single-body communication, the optimum is between 1.5 and 2.1MHz and for intra-body communication between 2 and 4 MHz. Higher frequencies have a fast slope downward in terms of attenuation and are worse in that regard.

The effect of using either one or two electrodes in the transmitter is modelled in [11]. In that work, the conduction currents that are induced between the two electrodes provide an electric field which is modelled in a simple rec-tangled shape. The methods used for these models are Method of Moments (MoM) and Finite Difference Time Domain (FDTD). From this research, it is concluded that by adding a ground electrode (moving from CC to GC), the electric field strength is stronger and thus, the received voltage strength is as well. The same relation between using a ground electrode touching the body in the transmitter is modelled in [57]. The modelling of the ground electrode in the transmitter makes the coupling a mix of GC and CC because the transmitter is then following the GC type of BCC. Since the receiver is not using a ground electrode that touches the human body, the receiver is operating according to the CC type of BCC. This latter research highlights the importance of keeping surrounding signal sources in mind because these easily interfere in systems using CC as a coupling method. The model built allows for analysis of interference in the surroundings from 0 to 250kHz.

Paper	Coupling	Model type	Frequency region	Inter-body
[3]	CC & GC	e.c.	10 kHz - 1 MHz	no
[11]	mix	MoM, FDTD & e.c.	0 - 100 MHz	no
[19]	GC	e.c.	200 kHz - 10 MHz	no
[35]	CC	FEM & e.c.	1 - 100 MHz	no
[49]	CC	e.c.	0 - 100 MHz	no
[2]	CC	e.c.	10, 21 & 100 MHz	no
[22]	GC	e.c.	200 kHz - 6 MHz	yes
[31]	CC	FEM	20 - 150 MHz	no
[30]	CC	e.c.	10 MHz	no
[24]	CC	e.c.	100 kHz - 1 MHz	no
[1]	GC	FEM	10 kHz - 1 MHz	yes
[29]	CC	e.c. & FEM	100 kHz - 1 GHz	yes
[57]	mix	e.c.	0 - 250 kHz	no
[58]	CC	e.c. & FEM	1 - 10 MHz	yes
[26]	GC	e.c. & FEM	0 - 1 MHz	no

Table 2.2: **Overview of research using models of the body channel**

2.3 Privacy

One of the main reasons for using Body Coupled Communication (BCC) is its capability of providing a private communications channel. Private, since intercepting the signal becomes hard without touching the body, to which the signal is coupled. BCC was first introduced by Zimmerman in [60] and already in his paper, one of the first reasons mentioned is: "A low-frequency carrier (less than 1 megahertz) is used so no energy is propagated, _minimizing remote eavesdropping and interference by neighbouring PANs", in which PAN stands for "Personal-Area-Network". The focus of this work is on providing a reliable communications channel to support the possibility of a private channel. As is seen in evaluations later on, and shown by other related works previously mentioned, lower frequencies are worse in propagating through the body compared to higher frequencies such as those around 80MHz-90MHz[41]. For that reason, the modulation scheme must be robust and (Frequency Shift) Chirp Spread Spectrum Modulation (FSCSSM) is proposed as a method to provide such a robust modulation scheme.

In his work[60], Zimmerman states that the use of near-field communication is the ideal solution and that this suggests operation frequencies between 0.1 and 1MHz. Why that is, he doesn't mention and neither does he explain what those values are based on. In a broad survey ([41]) the argument of radiation is found and stated that the frequencies should be below 300MHz for it not to radiate due to the wavelength having about the same length of the body channel. The frequency of 300MHz, however, was one of the largest estimations found for a private channel, especially compared to the frequency region mentioned by Zimmerman in [60]. In [6] (Capacitive Coupling (CC)), a calculation is provided to obtain a threshold frequency for leakage. The frequency threshold indicates a frequency above which "the leakage signal out of the human body is picked up in the air medium"[6]. This frequency threshold is 23.88MHz.

It was mentioned already in the previous section that in [29], Nath et al. looked into using another body as a capacitive coupler to pick up the signal from another body. This is possible since two bodies can couple together in terms of capacitance. The capacitance is found about 80pF at 10cm and decreases (not linearly) to less than 10pF at 5m. Their work states that at least an SNR of 5dB is required at the receiver. When the rightful receiver was intended to receive a signal with an Signal-to-Noise Ratio (SNR) of 30dB, the snooping device at a 5m distance received less than 5 dB. However, at 10cm the intended device still received a signal with SNR of about 25dB. When the intended SNR was 10dB, it was received as about 4dB at the snooping device at 10cm. Sending signals with a low SNR helps prevent attackers from picking up and successfully decoding the signal. That is if 5dB indeed is the valid threshold. In FSCSSM this is not the case since that modulation can operate below the noise floor of 0dB (SNR). In their research it is shown that however strong the SNR at the transmitter might be, the decay over distance has the same slope. Given that, an estimation could later be based on this slope for at what difference the signal can be sniffed for this thesis. Different from this thesis is that their work is based on a capacitive coupling method and also higher SNRs are required to decode a message successfully. The latter is not the case as this thesis is targeting to decode signals below the noise floor.

Most research into sniffing attacks is provided for CC as a coupling method. Just as the previously mentioned research. Tomlinson et al., however, did research the possibility of a side-channel sniffing attack on a system based on Galvanic Coupling (GC) in [45]. In their work, the over-the-air effects were tested up to 15cm for both GC, CC and a combination of the two. It was found that GC was less susceptible to sniffing compared to CC. At a distance of 13cm, the system making use of GC hit the noise floor for the sniffing device. The transmit power applied in their evaluation is, most likely, -2dBm. The latter is important but not explicitly stated for the over-the-air evaluation in their paper.

Given the research performed by Tomlinson et al.[46] on GC that concludes that GC is less prone to leakage than CC with about a 15 to 20dBV difference and that CC is already hard to sniff for low SNR at short distances.

2.4 Noise

When the focus is placed on designing a system that provides reliable communication, it is useful to have an estimation of what noise levels are present inside the channel and to verify how other research has approached communications with (highly) noisy channels.

The noise present in the human body was measured by Varga et al. in [48]. They measured Signal-to-Noise Ratio (SNR) for the frequencies 2, 4 and 8 MHz in various locations. The measurement was performed by measuring the signal on a device on various parts of the human body, transmitted by another device on the body for which both used Capacitive Coupling (CC) as coupling method. In their work[48], it was found that 8MHz centre frequency achieved a lower SNR for communication compared to 2 and 4MHz with 2 being the worst (highest) SNR. For the 2MHz signal, they provided measurements where a 0dB SNR was found. This would mean that the body channel was highly noisy and the received noise had an equal amount of average power as the original signal. Most modulation schemes would not be able to recover a signal when receiving a signal of 0dB SNR. For the same subject, the SNR on 4MHz was about 18dB (graphical estimation), indicating that a higher centre frequency is attenuated less.

Using these measurements, for lower frequencies ($< 2MHz$), it is found that the channel can be very noisy and with the privacy perspective in mind, a communications scheme that is prone to noise is suggested. However, these conclusions were found for channels making use of CC while this thesis proposes Galvanic Coupling (GC).

Wegmueller et al. performed measurements on a channel using GC[52]. They found that, on a short distance the achievable SNR was 37dB at best. A measurement on the thorax gave them a measurement of 26dB SNR at best. The electrodes used were electrodes using a sort of gel enabling higher interactivity with the body. This could be beneficial in short-term medical environments but not for daily wearables. The Shannon Channel Capacity theorem is applied in their paper stating that, for the achieved SNR of 37dB at a bandwidth of 100kHz and a centre frequency of 200kHz, a data rate of 1.26Mbps can be achieved. A keynote must be placed that for this evaluation, the electrode sizes were quite large sizes which is not practical either. about $560mm^2$. For medical applications or daily use, a maximum of $100mm^2$ is more likely, achieving a lower SNR.

2.5 State of the art

Currently, there are not a lot of works having prototypes with the use of Galvanic Coupling (GC) as a coupling method. The works that are, have been listed in the table below.

Work	Year	Interbody	Frequency	Data rate
[53]	2012	no	$50kHz, 100kHz$	$5kbps$
[50]	2014	no	$125kHz$	$100kbps$
[48]	2018	yes	$8MHz$	$3.5kbps$
[7]	2016	yes	$10.7MHz$	$9.6kbps$
[8]	2021	yes	$10.7MHz$	$57.6kbps$

Table 2.3: **Related works comparable with this thesis**

From these works, not a single one can achieve communication below the noise floor. Data rates are not high either, but that is not expected to be improved by this work since noise is the main focus. Research in the table that tackles inter-body communication uses frequencies from 8MHz or above which is not looked into in this thesis. When a higher data rate is desired, other tradeoffs have to be made and most likely, Capacitive Coupling (CC) is more desired.

2.6 Frequency Shift Chirp Spread Spectrum Modulation

The theory of (Frequency Shift) Chirp Spread Spectrum Modulation (FSCSSM) is widely available but the known implementation of it is LoRa. LoRa is a communications method often used in Internet of Things (IoT) which stands for "Long-Range". As the name says, it offers very long-range communication possibilities which is mainly due to the implementation of FSCSSM. While FSCSSM is not only implemented by LoRa, it is the most known example of implementation and therefore a lot of research on FSCSSM is with regard to LoRa.

The theory found is mostly based on a few resources. In [47] the mathematic model of the LoRa (de-) modulation is proven, as stated by the author, for the first time. Their model is the basis of the modulation scheme implemented in this thesis. The theory section (Chapter 3.3) will refer to most of the equations provided in their work. In their research[47], only the mathematical orthogonality of chirps with different symbol values is provided but from those, one can deduct the mathematics for the dechirping process. These mathematics are more explicitly explained in [33]. The mathematics provided in [33] explain how the actual dechirping process is performed while the mathematics in [47] explain why the dechirping process is valid actually working. These works combined form the base for the implementation of FSCSSM in this thesis.

There is one more team of researchers (Knight and Seeber) that reverse-engineered LoRa-PHY, which is the physical implementation of LoRa[20]. In LoRa, a preamble is used as a repetition of chirps with the symbol value 0. According to [20], one such a chirp is not sufficient but "once de-chirped and passed through an FFT, a preamble may be identified if enough consecutive FFTs have the same argmax"[20]. That sentence is quoted since later in this thesis, it is shown that with the number of samples taken in this prototype such an implementation leads to too many positive false flags. It is also found in their work that LoRa implements a few extra features to increase the success rate of symbols. Gray-coding is implemented to prevent off-by-one errors and whitening is applied to introduce extra randomness for clock synchronisation. The most relevant of extra implementations is the addition of Forward Error Correction (FEC). In LoRa, a Hamming FEC is applied such that the receiver has additional information to verify and potentially correct the received signal. Adding a means of FEC could increase the success rate of the transmission.

Dechirping the chirp into a symbol can be done using either multiplication and performing a Fourier Transform (FT) as is performed in [20], [47] and [33] but can also be done using a correlation which is done by [21]. The correlation is, however, more inefficient since for each potential symbol (the amount depends on the spreading factor), a correlation has to be performed with the received signal. What's more, is that the multiplication in the dechirping process is a multiplication with another default waveform. In [20] this is called a down chirp, in [47] this is called the complex conjugate of a pure upchirp. A pure upchirp has a symbol value of 0, so no shifting has taken place. This multiplication is a multiplication with the base down chirp. However, various researchers use different terminology. In [33] it is found that this is referred to as the complex conjugate of a pure up-chirp. In [20] this is called a down chirp and in [54] its called a "base down chirp".

From these works, also various namings for FSCSSM are used. [20], [54] and [33] use "Chirp Spread Spectrum Modulation" and [21] and [47] use "FSCM" which means "Frequency Shift Chirp Modulation". In this thesis, it is decided to use (Frequency Shift) Chirp Spread Spectrum modulation. The part "Frequency Shift" emphasizes the actual cyclic shift in the frequency domain to modulate a given symbol, while "Chirp Spread Spectrum" indicates the spreading of a signal over a bandwidth of frequencies forming a "chirp".

With respect to noise and Signal-to-Noise Ratio (SNR), of the referred works here, [33], [47] and [54] do evaluate the effect of FSCSSM. In [47] the Bit Error Rate (BER) is compared between FSCSSM and Frequency Shift Keying (FSK) for multiple SNR levels. It was found that FSCSSM outperforms FSK in frequency selective channels (such as the human body). In [54] simulations estimate that LoRa can operate up to -20dB SNR (for an Spreading Factor (SF) of 12) which indicates that this modulation scheme allows for operation below the noise floor. In [33] the same conclusion is drawn where multiple

spreading factors are compared to each other on SNR versus symbol error rate.

While these works each contribute to LoRa with new modulation and demodulation proposals, for this thesis, the most relevant sections are the theory on FSCSSM. For more robustness, the referred research can be applied to strengthen this thesis' implementation in future work.

2.7 Safety

In Body Coupled Communication (BCC), an electromagnetic signal is coupled to the human body. Safety is of the essence. By using battery-operated devices, Wegmueller et al. guarantee that the devices are not connected to mains power thus preventing any dangerous voltages into the system [51]. The devices need to be electrically separated in this thesis to prove operation on battery-operated devices. By applying this idea to the transmitter prototype in this thesis, their safety measure can be adapted.

As is stated by [59], at these frequency levels the most obvious effect is (tissue) heating. In addition, from [59] it is found that the system may not induce current or apply voltages above levels stated by IEEE Std. C95.1 2019 [16] and International Commission on Non-ionizing Radiation Protection (ICNIRP) guidelines [15]. From these regulations it is concluded, by [59], that The maximum harmless induced current in BCC should be lower than 20mA at a frequency range of 100kHz to 110MHz.

2.8 Conclusion

From all the research on Body Coupled Communication (BCC), of which only the ones most important were mentioned here, it is found that Galvanic Coupling (GC) is not the most commonly known coupling type mostly due to the lack of data rate. Due to the lack of data rate, a lot of works discard the privacy argument for which BCC was intended by Zimmerman ([60]) in 1996 in the first place. Besides privacy, the noise aspect is barely looked into either. The focus of the thesis is therefore to transmit at low signal strength, through a highly noisy channel by using (Frequency Shift) Chirp Spread Spectrum Modulation (FSCSSM) in BCC.

The body channel is found to be frequency selective and noisy. As was found by the research on FSCSSM, the modulation scheme FSCSSM allows for operation below the noise floor and does outperform other modulations such as Frequency Shift Keying (FSK) especially in frequency selective channels.
Moreover, FSCSSM is used in long-range applications which could have a positive effect in a channel with high attenuation.

The demodulation process of FSCSSM could be inefficient when cross-correlating all possible symbols but a mathematical trick allows efficient demodulation with the use of a multiplication followed by an Fourier Transform (FT) while undersampling the received signal. Compared to the signal length, very few samples are required and the effort of demodulation is limited which results in a (power) efficient system.

Chapter 3

Theory

The theoretical description of the key components used in this work is described in this chapter. Theory on the modulation scheme used and the electrical characteristics of the receiver circuit is provided and explained.

3.1 Body Coupled Communication

In Body Coupled Communication (BCC), a signal is transmitted by coupling a signal to the body. For coupling a signal to the body, three main methods have been provided by research. The three methods are Galvanic Coupling (GC), Capacitive Coupling (CC) and Magnetic Coupling (MC). Between GC and CC, there is the most similarity. The three methods have been depicted in Figures 3.1, 3.2 & 3.3.

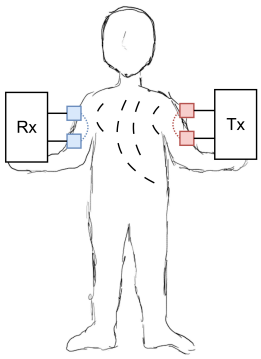

Figure 3.1: **Galvanic**

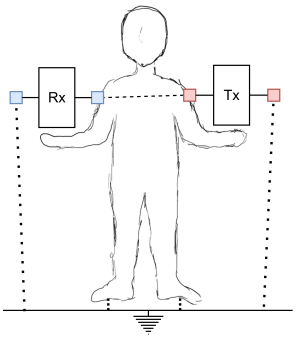

Figure 3.2: **Capacitive**

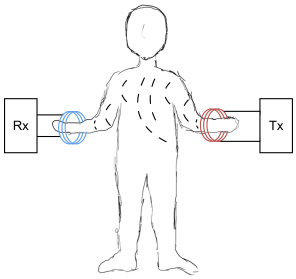

Figure 3.3: **Magnetic**

3.1.1 Galvanic Coupling

In Body Coupled Communication (BCC) using Galvanic Coupling (GC), the human body is used as a waveguide. A wave-guide poses a medium in which an Electromagnetic (EM) wave can propagate (is "guided"). Two electrodes, per device, are touching the body, with some spacing between the electrodes (inter-distance). This setup is depicted in Fig. 3.1. The two electrodes are provided with a potential difference (voltage difference) across them by having one of the electrodes equal to the transmitter's ground potential or other reference potential and the other electrode having a modulated potential voltage. The modulated signal has a potential voltage changing according to the modulation scheme which is (Frequency Shift) Chirp Spread Spectrum Modulation (FSCSSM) in this work. The potential difference applied across the two electrodes creates an electric field within the body, driving the flow of electric current through the body tissues. The field is initially created just like in a capacitor. This field

forms a path for a (small) current to flow through the body to receiving devices. This is depicted in Fig. 3.4, where points A are the transmitter's electrodes and points B represent the receiver's electrodes. The other way around, for the receiver, an electric field between two points will create a potential difference across the two electrodes.

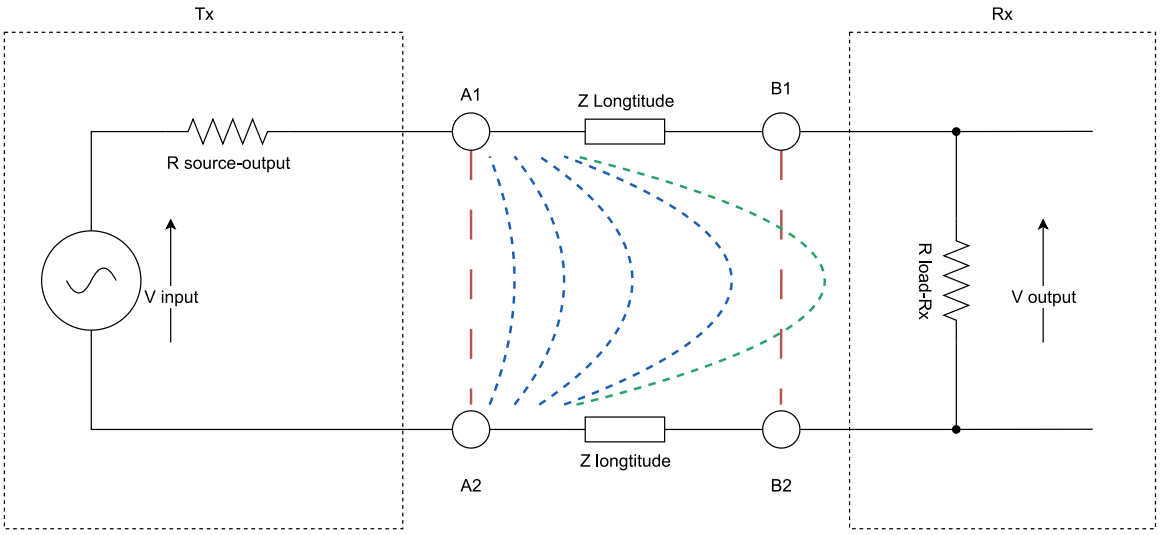

Figure 3.4: **Simple electrical model of the human arm for Galvanic Coupling. [18]**

$$E^*_{Tx} = \frac{V_{Tx}}{d \cdot \varepsilon} \tag{3.1}$$

$$V^*_{Rx} = E_{Rx} \cdot d \cdot \varepsilon \tag{3.2}$$

The (total) Electric Field strength between the two electrodes of a transceiver can be calculated by Eq. 3.1, where V is the applied potential voltage difference across the two electrodes, d the distance between them and ε is the permittivity of the body in that distance voltage across the electrodes. The unit of E is V/m. In reverse, the potential voltage difference across the receiver electrodes can be calculated by Eq. 3.2 where E_{Rx} is the electric field strength between the receiver's electrodes, propagated from the transmitter throughout the human body. It must be noted that the field has spread out across the body exponentially and also parts of it have leaked out of the body, so $E_{Rx} \ll E_{Tx}$ (E_{Rx} is way smaller than E_{Tx}). An important sidenote to both Eq. 3.1 and Eq. 3.2 is that these formulas are very simplified. In addition to the electric field creating a potential difference across the two electrodes of the receiver, an electric current flow enters the receiver as well. This current flow was possible due to the electric field created by the transmitter.

The potential difference is altered according to some encoding of the message that is supposed to be transmitted using this method. EM waves transport EM energy from the transmitter to the receiver like this, with the human body as the propagation medium. The propagation speed of that wave is about the speed of light. The receiver can either use one signal electrode or a signal electrode in combination with a reference (ground) electrode touching the body. Any received potential difference with the reference is decoded into a payload. Depending on the purity of the received energy, the decoded payload is correct or not. Energy from other sources might cause interference. However, since most of the energy is directed into the body and no floating ground reference is required for this method, GC is less susceptible to interference than, for example, Capacitive Coupling (CC). The current that is flowing from the signal electrode to the reference electrode on the transmitter, however, is a very small current and therefore, the created EM wave is weak. This might cause issues with the noisy human body as a communications channel. The medium, through which the signal is propagating, is the human body. The electrical characteristics in terms of resistance, inductance and capacitance, differ throughout the body and per layer of the body. For that reason, since nobody is the same, the signal behaves differently

in different bodies. To understand better what is happening, models have been composed that describe the electrical characteristics of the human body in terms of impedance, based on research. A basic model explaining the prior theory is found in [18] and is depicted in Fig. 3.4.

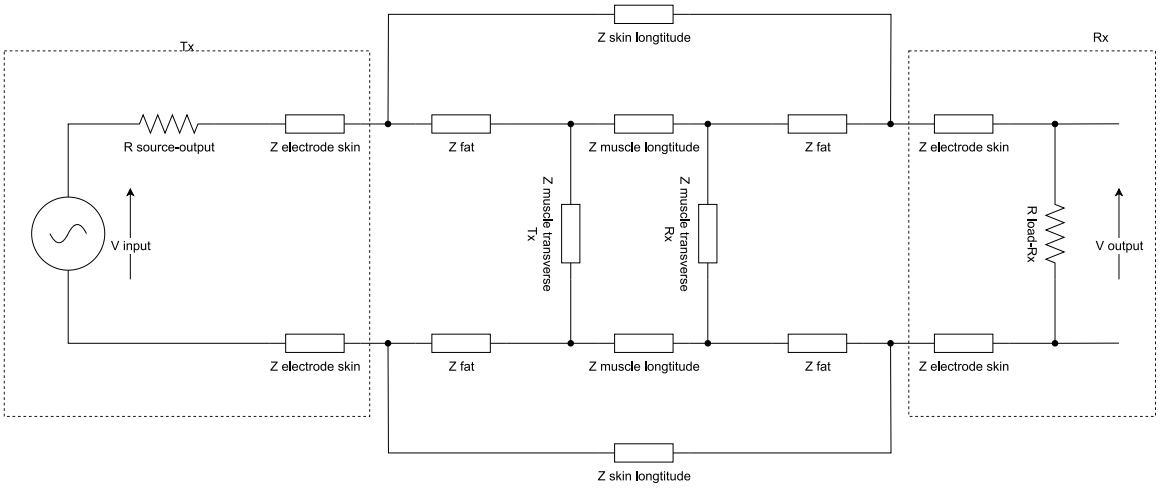

Figure 3.5: **Advanced electrical model of the human arm for Galvanic Coupling. [18]**

In the figure, electric-field-intensity (current-density) vectors are used to represent current flow paths in GC. The body is simplified in this model but in Fig. 3.5, a more advanced model is depicted that takes into account multiple layers of the human arm. Please note that bones have not been used in this model and neither the longitudinal characteristics of fat. The reason for not taking into account these characteristics is that their impedance was found to be very high in comparison with the other factors in this model, so they would not contribute to signal propagation.

3.1.2 Capacitive Coupling & Magnetic Coupling

The coupling method Capacitive Coupling (CC) is the most used coupling method in research, which is also referred to as "electrostatic" coupling. The reason for that is that the signal is attenuated less in the body when CC is used[10]. One electrode touches the human body and the other electrode is pointed away from the body. The signal electrode that touches the human body couples an Electromagnetic (EM) signal into the body. The other electrode is a reference electrode. The reference electrode is often the device's ground potential and is meant to couple with earth-ground "through the air". Coupling "through the air" creates a capacitive reference. This is depicted in Fig. 3.2. Since the human body does the same and the receiver does so too, a potential voltage reference is established on all components in the system. When the signal electrode changes its potential voltage (data modulation), a potential voltage difference, across the signal electrode and earth-ground, causes an EM field inside the body. The field is measured by the receiver and so changes in the field are picked up and demodulated back into meaningful data. Just like a model exists for Galvanic Coupling (GC), an electrical model was created for the signal propagation in CC. This model is depicted in Fig. 3.6.

In the model depicted in Fig. 3.6, the human body is simplified with a resistor and a capacitor in parallel. These components form the impedance that the signal is subjected to. Depending on the location of the transmitter and/or receiver device(s), the body characteristics could change a bit with, for example, added leakage capacitance with earth-ground. The capacitance in parallel with the resistance forms impedance together. The impedance description of this model, which was provided by both [35] and [58], can be elaborated more into the layers of the human body just like the model from GC depicted in Fig. 3.5.

Another method for coupling the signal into the human body is Magnetic Coupling (MC). For this coupling to work, a coil is wrapped around tissue or a limb. In Fig. 3.3 a coil is wrapped around the arm, for example. Alternating current flowing through a coil will create an alternating magnetic field in

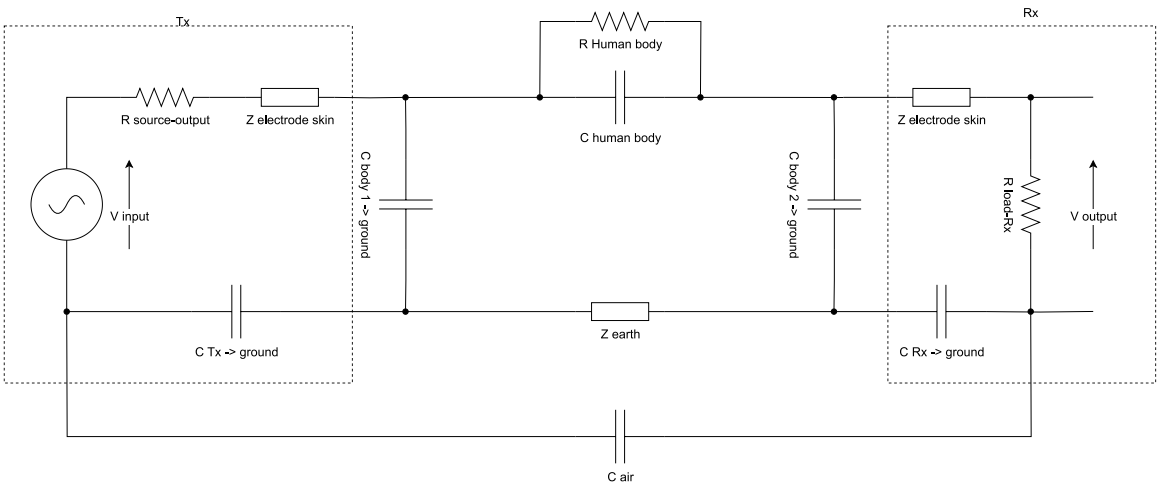

Figure 3.6: **Electrical model of the human body for Capacitive Coupling. [35] & [58]**

the coil. Because the human body (tissue) is the inside of the coil, the magnetic field will be coupled to the human body and so a receiver, configured in the same method using a coil, will be receiving a signal since a changing magnetic field in a coil will induce a changing electric current in the coil. The magnetic field strength in the centre of a coil is described by Eq. 3.3. Rewriting that equation for the receiver yields the current induced in the coil of the receiver in Eq. 3.4. The magnetic field strength in the centre of the receiver coil is described in Eq. 3.5. In these equations, N are the number of loops of the coil, μ is the permeability of the medium and R is the radius of the coil. Since the receiver does not receive the full strength of the transmitted magnetic field B, the receiver's magnetic field is described as factor η times the transmitted magnetic field, plus noise. The reason for not receiving the full strength of the transmitted magnetic field is due to the spreading of the field throughout the body and potential leakage. The strength-per-area of the B field reduces with an exponential factor per unit distance from the transmitter.

$$B = \frac{N\mu I}{2R} \tag{3.3}$$

$$I_{Rx} = \frac{2R * B_{Rx}}{N\mu} \tag{3.4}$$

$$B_{Rx} = \eta B_{Tx} + B_{noise} = \eta \frac{N\mu I_{Tx}}{2R} + B_{noise} \tag{3.5}$$

For this method of coupling, a practical downside makes this method obsolete. The device must always manage to wrap a piece of tissue or limb with multiple conducting loops making a full electrical connection.

3.2 Potential Reference

Communication between devices is established by transmitting electrical signals. These signals are picked up as a potential difference with respect to another potential reference voltage. Often, in wired communications, for example, two wires are used and a potential difference across them is created by the transmitter. The receiver picks up that difference by measuring the potential difference across the two wires. The receiver can consequently decode the transmitted signal. In wireless communication, the air or transmission medium will act as just one of those wires. The other wire, the reference, is either a shared ground or, often in battery-based devices, the alternating signal is referenced to a potential based on the device's battery. Body Coupled Communication (BCC) is practically the same as wireless communication in that sense that there is one "wire" (the body). The picked-up signal will be a potential difference across the receiver electrode and the receiver's potential reference electrode. The receiver's potential reference electrode is (often) directly electrically connected to the battery's negative terminal.

Electrically speaking, energy in electrical signals is not in the wires but between the two potentials. Having both a signal wire and a reference wire (ground) means that the energy is transported between those wires to the receiver and most of the energy is contained. In wireless communication, the energy spreads in all directions, not focusing its energy in one direction, and so the receiver will have to deal with a weaker signal in the first place. That is why in BCC, the circuit needs to be designed such that any slight changes in energy (data) are amplified and received. During evaluation, the devices must be electrically separated to ensure the operation of communication when, for example, battery-operated devices around the body are used in applications.

3.3 Frequency Shift Chirp Spread Spectrum Modulation

A more steady communication can, in theory, be established using the properties of (Frequency Shift) Chirp Spread Spectrum Modulation (FSCSSM) in Body Coupled Communication (BCC). Why that is, is explained here. In FSCSSM, the transmitted signal is spread out over a bandwidth to allow for a very advantageous Signal-to-Noise Ratio (SNR). To understand why that is, first, a few terms in this method are addressed.

The "C" in FSCSSM stands for "Chirp". In FSCSSM, data is modulated into an analogue electrical signal. That signal is formed by creating an alternating current with linearly increasing frequency over a period of time. The frequency is "swept" over time through the available bandwidth.
As an example, when the bandwidth is $20kHz$ and the centre frequency is $100kHz$, all frequencies used in the sweep have a value between $90kHz$ and $110kHz$. The actual frequencies used in this work are different and explained later. If such frequency sweep had been performed in the audible frequency range using sound waves (moving air particles), the human would hear a so-called "Chirp". That chirp would be a sound changing from a low to a higher frequency over a period of time. However, because this kind of frequency sweep in the audible range sounds like a chirp, is not the main reason for it to be called a chirp. Chirp is an abbreviation for "Compressed HIgh-Resolution Pulse". The signal is a sweep of frequencies starting at the centre frequency minus half the bandwidth and ending at the centre frequency plus half the bandwidth.

Chirping is used in radar technology because it forms a compromise between sending a single-frequency waveform and a "perfect" delta function. Single-frequency waveform makes it hard to distinguish multiple targets on the radar since multiple reflections have various delays of which correlation might overlap. On a low-power signal, noise added to this signal makes it even harder to measure delay. A filter in the frequency domain would show a narrow-band waveform. When using a delta function pulse as the signal, the power would have to be instantaneous and very high which is hard to achieve. This would, however, provide the ability to distinguish multiple targets that are located close together. An ideal delta function would include all frequencies equally in the frequency domain, a wide-band signal. A chirp signal results in a wide-band signal (not as wide as the delta function) and a low-power signal (power is spread out over time). Plus, correlating the chirp yields a very narrow peak allowing for high distinguishability and because of that, the signal is robust against noise.

This chirping was visualized in the introduction and is once more depicted in Fig. 3.7. The figure shows how a chirp signal will look in amplitude over time and how the frequency increases linearly over time. Note that this is purely a visual example and not a representation of the real frequencies and time periods used in this work.

When a receiver applies a matched filter on the received signal, the peak of correlation would be narrow and high. This cross-correlation of a received signal with a matched filter, over time, is displayed in Fig. 3.8. Only when the signal fully overlaps the matched filter (reference signal), does the correlation peak. This indicates that another signal received a little later or earlier in time can be easily distinguished from another signal.
Chirping itself, however, does not directly pose a method for encoding and decoding (modulation and demodulation) your message but it is merely a method used for the transport of your message. The logic behind FSCSSM is that a cyclic frequency shift can be applied to the chirp to pose a set of bits. The

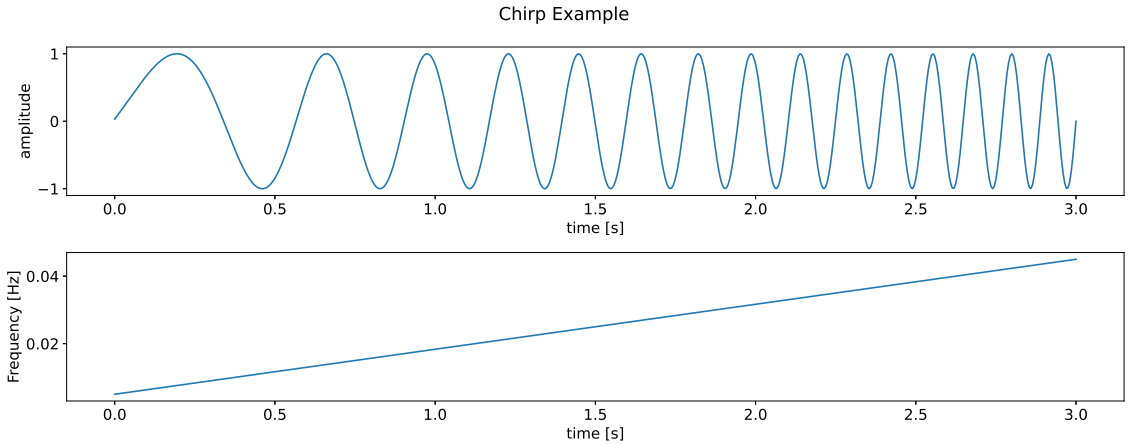

Figure 3.7: **Example of a chirp and its frequency behaviour**

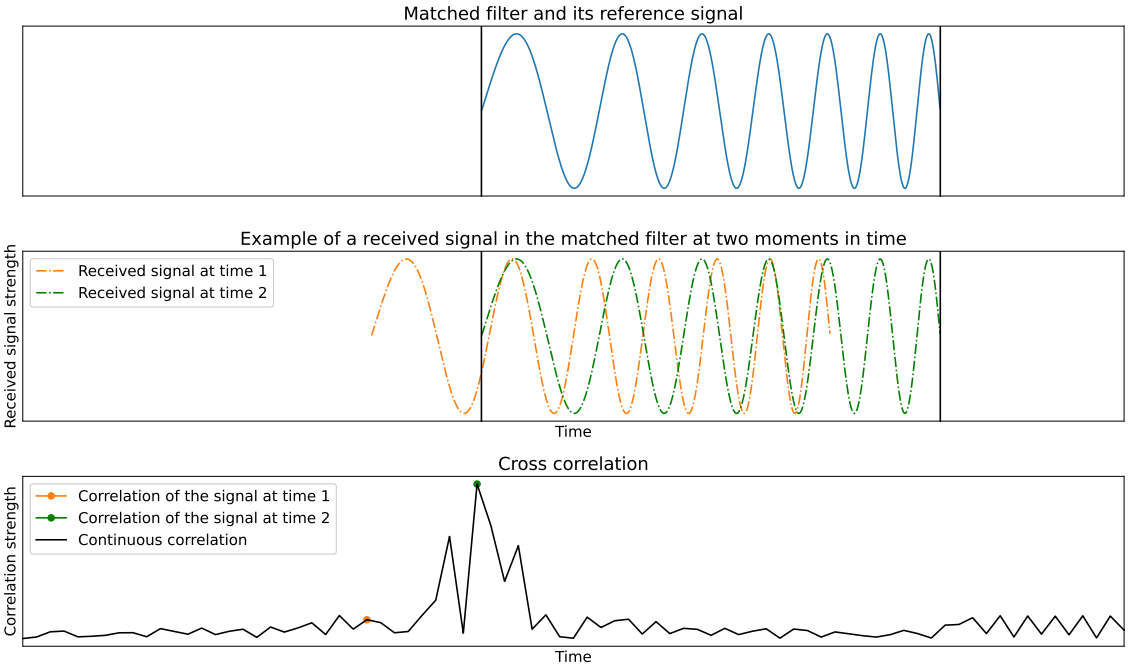

Figure 3.8: **Cross-correlation between a matched filter and a received signal at multiple moments in time.**

amount of frequency shift is the modulation technique applied. A cyclic shift means that a part at the end of the chirp (as depicted in Fig. 3.7) can be moved to the front of the chirp. This would result in a chirp that looks like the one in Fig. 3.9.

The number of bits, or possible cyclic shifts, possible in FSCSSM is given by the so-called Spreading Factor (SF). The SF indicates in how many chunks the chirp is divided and for how long one chirp will last. Such a chunk is what is called a "chip". Each chirp has 2^{SF} chips. For example, if the SF equals 3, the chirp can be cyclically shifted into 8 different positions to represent a value from 0 to $2^{SF} - 1 = 7$. Each one of those 8 different positions can be transmitted. The chirp that is shifted into one of those positions is called a "symbol". So when the SF is 3, the symbol value of a chirp can be one from the set $\{000, 001, 010, 011, 100, 101, 110, 111\}$. Each shift has the size of one chip from a time perspective.

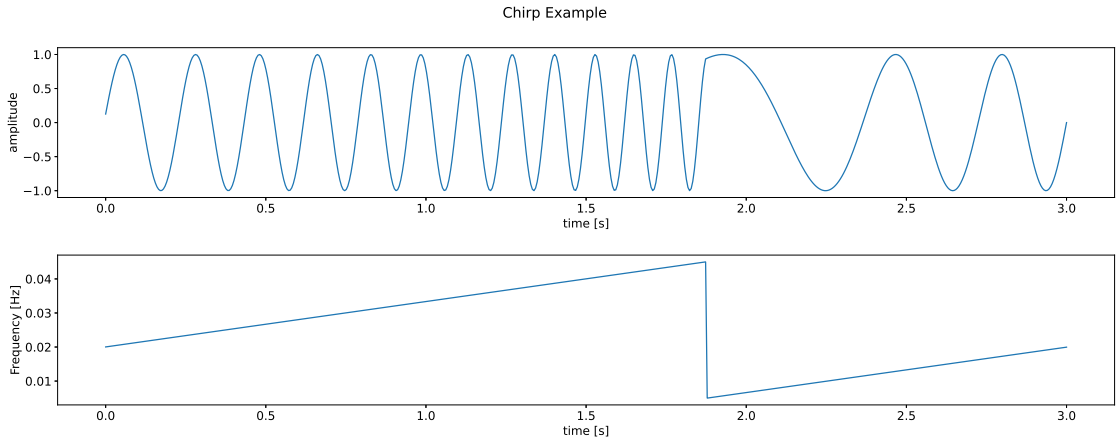

Figure 3.9: **Example of a chirp and its frequency behaviour, after a cyclic shift**

$$N = 2^{SF} \tag{3.6}$$

$$T_{chip} = \frac{1}{bandwidth} \tag{3.7}$$

$$T_{chirp} = N * T_{chip} = \frac{2^{SF}}{bandwidth} \tag{3.8}$$

The number of chips, which is equal to the number of different values the symbol can have, is N as provided in Eq. 3.6. The total duration time of one chirp is determined by the amount of chips in the chirp. The duration of one chip is given by Eq. 3.7 which yields the duration of the whole chirp to be calculated with Eq. 3.8. Eq. 3.8 indicates that a larger bandwidth will reduce the chirp duration and a larger spreading factor will increase the chirp duration. The logic behind those duration times can be explained. When the bandwidth is increasing, the frequency differences between chips are increasing as well. There is less necessity for spreading information over time because there is a more notable difference between chips. However, when the spreading factor increases, the time over which the amount of chips (which is also increasing according to Eq. 3.6) are spread needs to be increased as well. That is because to keep the same level of distinguishability between chips, each chip's duration should not decrease for the same bandwidth and so each extra chip adds up one T_{chip} to the total chirp time T_{chirp}.

Assuming that the SF (and thus N) is given, the receiver should correlate each incoming chirp with N potential chirps. Each of those possible chirps to correlate with is representing one out of N symbols. Fig. 3.7 and Fig. 3.9 are a visual example of two chirps each with different symbol values. It has to be noted, however, that N increases exponentially with an increasing SF. For a larger SF, the receiver must correlate the received chirp with a large number of potential symbol values. Doing so is a computationally expensive task so an easier, faster and less power-consuming method is useful. Using a mathematical trick, as explained in [47], under-sampling the chirp by taking N samples, multiplying those samples with a "down-chirp" and submitting those multiplied samples to an N-Point Discrete Fourier Transform (DFT) will yield a peak at the frequency equal to the transmitted symbol value. In Fig. 3.7 a so-called "up-chirp" is depicted. A down-chirp is a chirp starting at a high frequency and ending at a lower frequency. That is simply an "up-chirp" flipped around its x-axis in the figure. However, in the real world, there is a bit more complexity to it. The down-chirp is the complex conjugate of an up-chirp. The up-chirp is a chirp with a symbol value of zero.

The maths that allow the more efficient algorithm to work, assume that all signals are complex analytical signals. The depicted signals in Fig. 3.7 and Fig. 3.9 are not complex signals, they are "real" signals

without any "imaginary" component. A receiver could either sample both I/Q signals, In-Phase(I) and Quadrature(Q), or sample the incoming signal at Nyquist Sampling rate ($F_s \geq F_{max}$) and apply a Hilbert-Transform to acquire the complex analytical signal.

$$c(nT_s + kT) = \frac{1}{\sqrt{2^{SF}}} e^{j2\pi[(s(nT_s)+k) mod\ 2^{SF}+k-k]kT\frac{B}{2^{SF}}} \tag{3.9}$$

$$c(nT_s + kT) = \frac{1}{\sqrt{2^{SF}}} \underbrace{(e^{j2\pi 2^{SF}k^2T\frac{B}{2^{SF}}})}_{\text{base up chirp}} \quad \underbrace{(e^{j2\pi[s(nT_s)]kT\frac{B}{2^{SF}}})}_{\text{a pure wave at frequency } s(nT_s) \text{ Hz}} \tag{3.10}$$

$$c(nT_s + kT)|_{s(nT_s)=0} = \frac{1}{\sqrt{2^{SF}}} (e^{j2\pi 2^{SF}k^2T\frac{B}{2^{SF}}}) \tag{3.11}$$

Provided in [47] is Eq. 3.9, which is an equation describing the chirp-value, in complex form, for symbol-value $s(nT_s)$ at sampling point k. In the equation for the symbol value $s(nT_s)$, s is the list of symbols to be transmitted in a package, for which the outcome is the symbol at the n^{th} symbol period T_s. This equation (3.9) describes the mathematics that can be applied to an under-sampled (complex) signal. The sampling rate, specifically, should be equal to $\frac{1}{B}$ in which B is equal to the bandwidth of the chirp. When N samples of the received (ideal) chirp are taken, the values of those N samples can be described with this equation by iterating over k. There is, however, one change made to Eq. 3.9 compared to how it is presented in [47]. This change is the addition of $[+k-k]$ which is equal to 0 and so the mathematical outcome of the equation is not altered. Although the outcome is not changed, this addition makes it possible to rewrite Eq. 3.9 into Eq. 3.10, without changing the definition and/or outcome. In Eq. 3.10 it can be noted that there are two parts to the equation of which one is a base up-chirp, a chirp with symbol value 0, and the other is a pure wave at frequency $s(nT_s)$ Hz, which is the symbol value of the chirp. A pure base-up-chirp is provided in Eq. 3.11 which is derived from Equations 3.9&3.10. Removing the base up chirp component from the received signal would leave a pure wave at frequency $s(nT_s)$ Hz (the symbol value) from which the frequency can be obtained using an N-point DFT.

Removing the base-up chirp can be achieved by multiplying the received chirp at N samples, sampled at rate $\frac{1}{B}$, with the base-down chirp. Similar to how Eq. 3.11 was obtained, Equations 3.12, 3.13 can be used to obtain the base-down-chirp described in Eq. 3.14.

$$c^*(nT_s + kT) = \frac{1}{\sqrt{2^{SF}}} e^{-j2\pi[(s(nT_s)+k) mod 2^{SF}+k-k]kT\frac{B}{2^{SF}}} \tag{3.12}$$

$$c^*(nT_s + kT) = \frac{1}{\sqrt{2^{SF}}} \underbrace{(e^{-j2\pi 2^{SF}k^2T\frac{B}{2^{SF}}})}_{\text{base down chirp}} \quad \underbrace{(e^{-j2\pi[s(nT_s)]kT\frac{B}{2^{SF}}})}_{\text{a pure wave at frequency } s(nT_s) \text{ Hz}} \tag{3.13}$$

$$c^*(nT_s + kT)|_{s(nT_s)=0} = \frac{1}{\sqrt{2^{SF}}} (e^{-j2\pi 2^{SF}k^2T\frac{B}{2^{SF}}}) \tag{3.14}$$

In summary, the receiver only needs to know the N values of a base-down-chirp, which can be calculated when the SF is known, to calculate the symbol value of the received chirp, using an N-point DFT. The N samples are taken with a sampling rate $F_s = \frac{1}{B}$ in which B is the bandwidth. The sampling rate is way smaller than the sampling rate required according to Nyquist so this is under-sampling.

A full summary of the sampling and dechirping process is visualized in Fig. 3.10. The figure shows the received signal, in which a frequency change is taking place after the 3^{rd} peak, indicating that the symbol value of this chirp is 1. The third waveform is the received signal, multiplied by the down chirp that is shown in the 2^{nd} waveform. These are all complex waveforms in the actual dechirping process, having a real and imaginary component.
For a Spreading Factor of 4, a total of 16 samples are taken of the multiplied signal, evenly spread. The samples taken are seen in waveform 3 and the wave they create is shown in the 4^{th} waveform. A sine-wave with a single frequency is the result of those samples and this wave is shown in the 4^{th} waveform of Fig. 3.10. The DFT of that sampled wave is shown in the bottom waveform of Fig. 3.10. The absolute

DFT peaks at 1, indicating that this received chirp has a symbol value of 1. Note that 16 samples are provided and the 4^{th} waveform shows 1 period for those 16 samples. For a chirp with symbol value 0, the samples differ very little in value and so their DFT becomes zero. Its process is visualized in Fig. 3.11 and for a chirp with symbol value 8, the visualization is given in Fig. 3.12. For all the representations, the amount of periods can be compared to the symbol value. When the symbol value is greater than half the amount of chips, greater than 8 in this example, the amount of periods visible in this view is no longer corresponding to the symbol value. The result of the DFT is actually based on the amount of turns that the phasor makes for the given set of samples.

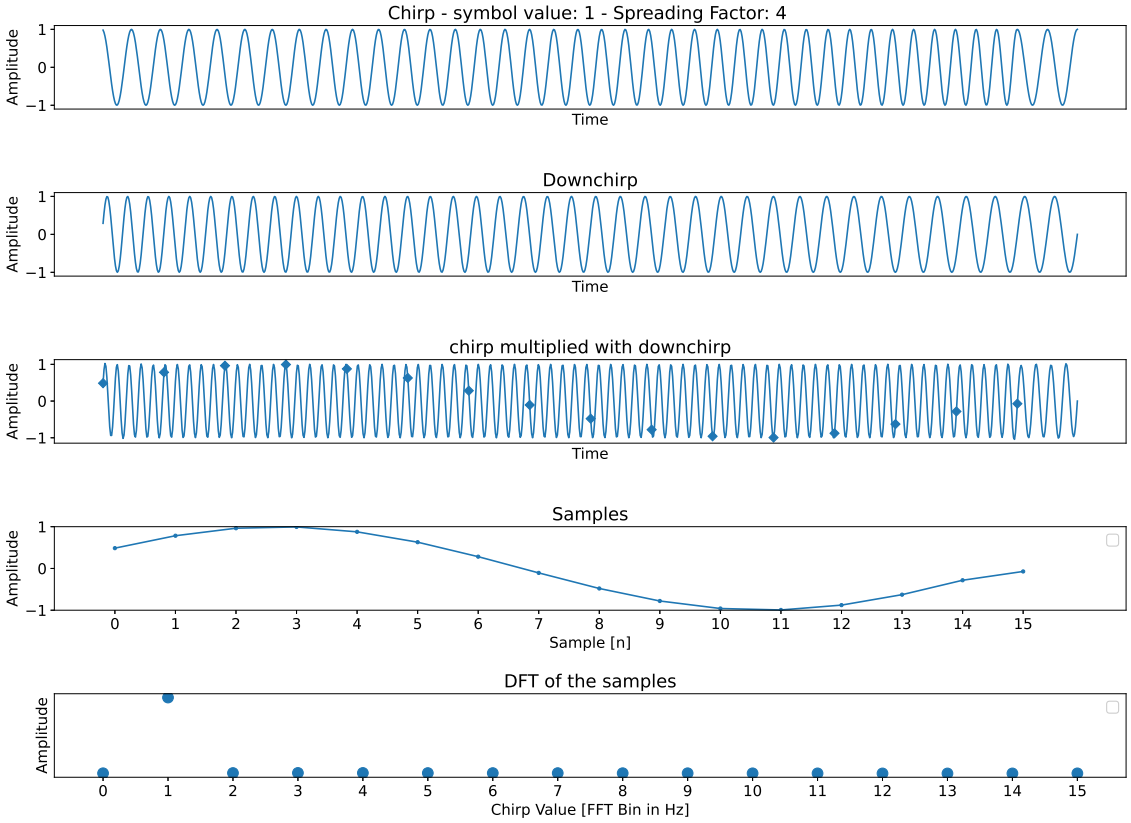

Figure 3.10: **Dechirping steps of a chirp with symbol value 1**

According to the work in [47], the received signal is described in Eq. 3.15 in which $w(nT_s + kT)$ is a zero mean white Gaussian noise, describing noise that can occur. The noise might be present, but as described is the spreading feature of FSCSSM allowing for a SNR below zero dB. The multiplication with the base-down-chirp of the sampled received signal is described in Eq. 3.16.

$$r(nT_s + kT) = \underbrace{c(nT_s + kT)}_{\text{chirp with symbol value } s(nT_s)} + \underbrace{w(nT_s + kT)}_{\text{White Gaussian Noise}} \tag{3.15}$$

$$d(nT_s + kT) = r(nT_s + kT) * e^{-j2\pi \frac{k^2}{2^{SF}}} \tag{3.16}$$

Effects on data-rate and Packet Error Rate (PER) are controlled by trade-offs in bandwidth usage and spreading factor. Changing the centre frequency does not directly result in different data rates or PER but might be beneficial for better performance given the channel the signal is propagating through. In the human body, it was found that a higher frequency results in better throughput, which is a matter elaborated on later. A decrease in bandwidth results in a longer chirp time but a longer chirp time does not directly mean better yields. The longer chirp time is a result of the mathematics required to make FSCSSM work with a decrease in bandwidth, given eq. 3.16. The upside of increasing bandwidth is that

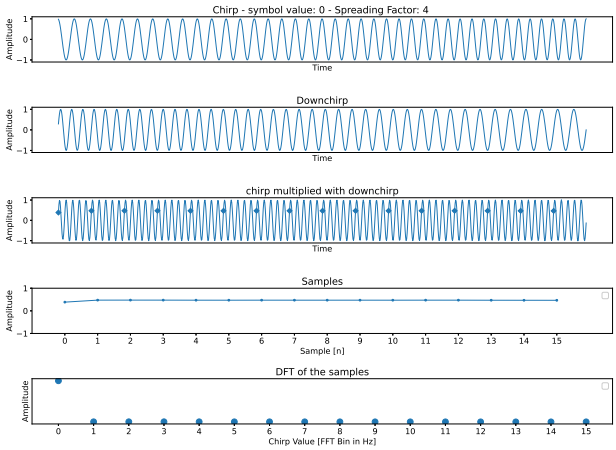

Figure 3.11: **Dechirping process symbol value 0**

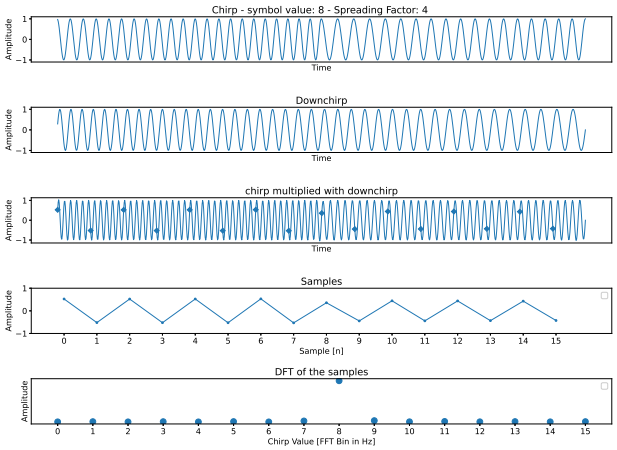

Figure 3.12: **Dechirping process symbol value 8**

frequency differences between the frequencies at sample intervals are more distinct. The greatest benefit is yielded by increasing the spreading factor, in terms of being prone to noise. Using Fig. 3.13, one can see that the use of a higher spreading factor yields different behaviour on the dechirped signal of a signal having symbol value 7. The result shown depicts that the absolute DFT in the dechirping process outputs a more flat and near zero result on frequencies that are not zero for a higher spreading factor compared to a lower spreading factor. Another result is that the amplitude of the DFT on the symbol value (7) of the signal is higher and distinct compared to those of lower spreading factors. Both the ideal situation (no noise is present) and the non-ideal situation (the SNR is -6dB) have been simulated and visualized in Fig. 3.13. The noise applied to each signal (all having a different spreading factor) is different since the signals all have a different structure due to their different spreading factors. This yields the visually different peaks or dips in the lines, seen in Fig. 3.13, in comparison with each other. Despite those different behaviours, the effect of the SF on noise resistivity is clear. A higher spreading factor in the modulation provides a more robust communication system.

The downside of increasing the SF, is that such an action would increase the Chirp Time and so the data rate will decrease according to eq. 3.8 and these effects are shown in Fig. 3.13.

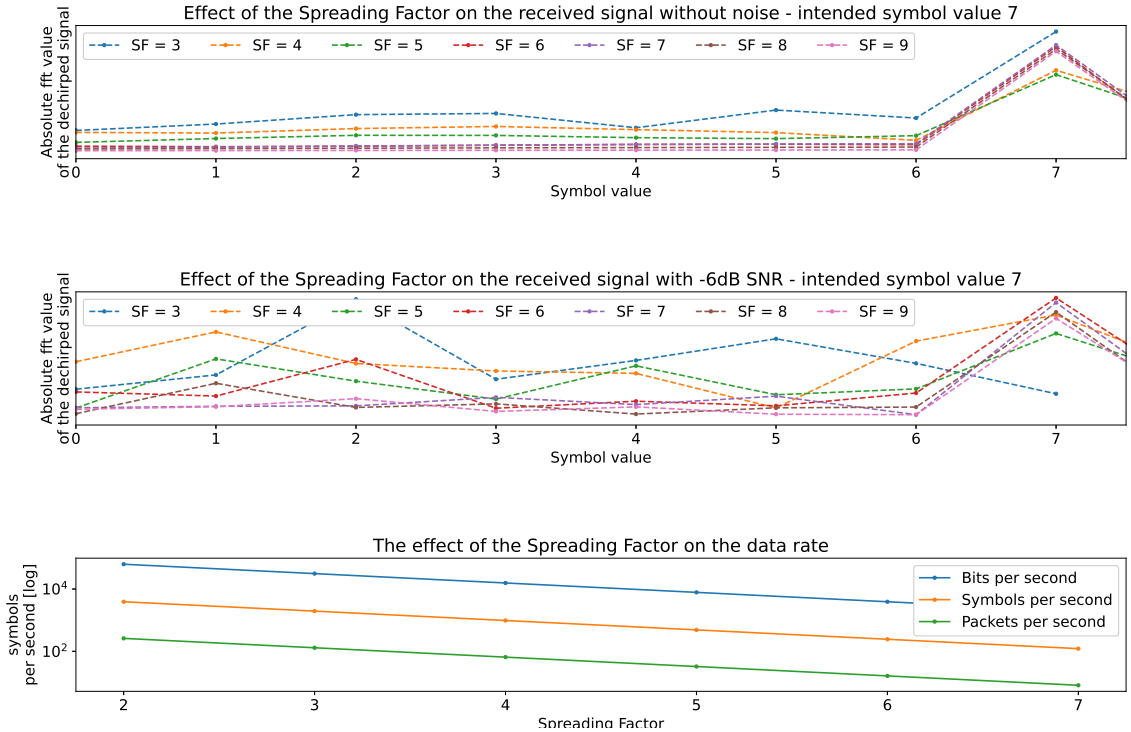

Figure 3.13: **Combination of the effects of spreading factor on an ideal signal, noisy signal and on the data rate**

Chapter 4

System Model

The prototype presented for this thesis is aiming to establish a private and most of all reliable form of Body Coupled Communication (BCC). Having such a form of communication could form a base for either new research into achieving higher data rates and/or real-life applications that require such private and reliable communications. In this section, the prototype model is described.

4.1 High level overview

In this work, data is to be transmitted from a transmitter to a receiver through a body channel using Galvanic Coupling (GC). The high-level overview can be split up into three parts which are, as depicted in Fig 4.1, the transmitter, the body and the receiver.

The transmitted signal is based on (Frequency Shift) Chirp Spread Spectrum Modulation (FSCSSM) which was chosen because of its (in theory) ability to be used below the noise floor. In the theory chapter (Chapter 3), the working principle is described and the parameters for FSCSSM are provided in the system model of FSCSSM.

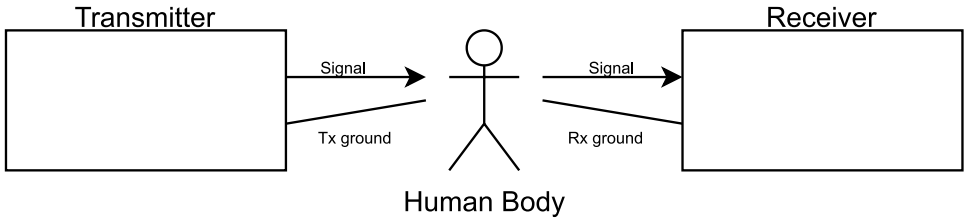

Figure 4.1: **High-level overview of the system model**

It is shown (in Fig 4.1) that, per device, two electrodes will touching the human body. Connecting two electrodes is done to meet the definition of GC which is making the system act like a wave-guide-based communications system, us the body as the medium or channel. What is important to note, is that the two ground signals are not shared ground. They could be, but common applications of this system would be battery-powered and do not share ground. The transmitter and receiver should be able to communicate without shared ground reference so this prototype is splitting the grounds to avoid misconceptions.

For both the transmitter and the receiver, a Field Programmable Gate Array (FPGA) is used to process the signals. The FPGA's used in this system both are the Nexys 2 Spartan-3E FPGA Trainer Board. The Very-high-speed Hardware Description Language (VHDL) design for these devices is written in a software called Xillinxs ISE 14.7. Reasons for using a FPGA are the relatively high sampling rates required in combined with the processing of those samples. Samples are taken in the order of microseconds. In this prototype, every time a sample is taken, a full Hilbert transform is applied on 128 samples fol-

lowed by the dechirping process. This cannot be achieved by using a (normal) microcontroller. For that reason, a FPGA is chosen since it can be completely optimised for this task and do parallel processing of those tasks at hand. The two systems are, as shown in Fig. 4.1, interconnected by the body as a channel or means of signal medium.

4.2 Transmitter

4.2.1 Body Coupled Communication

The transmitter creates a (Frequency Shift) Chirp Spread Spectrum Modulation (FSCSSM) based signal and couples it into the body using Galvanic Coupling (GC). In addition, the transmitter should not share common ground (potential reference) with the receiver. The transmitter consists of a Field Programmable Gate Array (FPGA) powered by a power bank to eliminate common ground. The FSCSSM signal is a 10-bit valued output of the FPGA which is connected to a Digital to Analogue Converter (DAC). The DAC chosen is a MAX5184BEEG+ by Maxim Integrated which has an option for 10-bit input. A DAC with, for example, Serial Peripheral Interface (SPI) is not desired since the update frequency would be too low to create a smooth wave at the frequencies chosen. The structure of the transmitter is shown in Fig. 4.2.

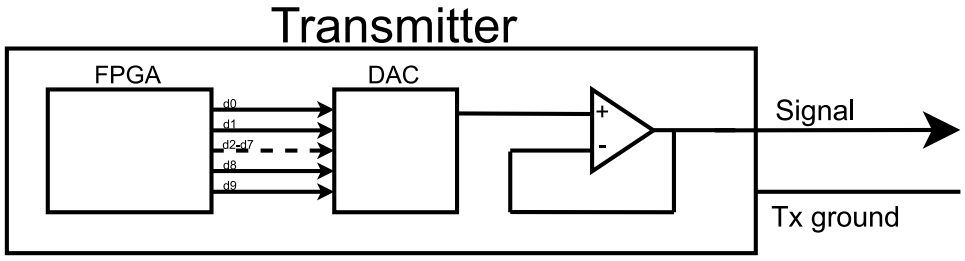

Figure 4.2: **High-level overview of the transmitter**

The analogue output signal of the DAC is subjected to a non-inverting Operational Amplifier (op-amp) configuration. The op-amp used is an OPA2863DR by Texas Instruments. This op-amp is a low-power, 110-MHz rail-to-rail amplifier allowing amplification from exactly 0V and the update frequency is sufficient for our application. Since the exact frequencies were unknown prior to this thesis, it is now concluded that an op-amp with lower frequency capabilities could be used when this would lead to more (power-) efficiency. The op-amp's gain can be set using a potentiometer which is the feedback resistor. Another fixed resistor acts as the ground resistor in the feedback circuit. The full schematics can be found in Appendix B.

The DAC is set up according to its datasheet. The output from the op-amp is twisted into a pair of wires with the other wire being connected to the transmitter's ground potential. The wires are connected to a pair of electrodes on a double-sided Velcro strap, forming the electrode pair for GC. The electrodes are two pieces of copper sheeting, cut into small rectangles

4.2.2 Frequency Shift Chirp Spread Spectrum Modulation

On the transmitter, the Field Programmable Gate Array (FPGA) creates a 10-bit signal that is fed to a Digital to Analogue Converter (DAC), yielding a single analogue signal. The 10 bits together form the chirp wave created by the FPGA. Each bit is provided with its own wire to the DAC along with a wire for the update signal on the DAC. More detail on how the output of the FPGA is generated, is provided in Chapter 5.

4.3 Body channel

The chosen coupling type is Galvanic Coupling (GC). This coupling method requires two electrodes per device of which one is the device's ground potential. The other electrode is used to transport the signal either from or towards the body. A human body is used as the channel.
Since GC is the chosen method for communications, the reference electrodes of both the transmitter and receiver should be connected to the human body. Devices that are intended to use a system like this are wireless and operating on battery. Using a battery means that, because there is no physical connection between the devices except for the human body, they do not have a common ground potential. In testing, devices should therefore be electrically isolated from each other to mimic such a scenario.

4.4 Receiver

4.4.1 Body Coupled Communication

The receiver has not only to perform the digital aspect of demodulating the received signal but it has to pick up an analogue signal from the body and perform filtering, amplification and the analogue-to-digital conversion on that signal before the digital aspect. An Analogue Front End (AFE) is designed for the prototype of this thesis to perform that task.
The electrodes touching the body are picking up not only the signal but also a lot of noise. The first step is filtering unwanted frequencies by applying a band-pass filter which is a combination of a High-Pass Filter (HPF) and a Low-Pass Filter (LPF) in series. The HPF only allows frequencies above the set cutoff frequency to pass and the LPF does the opposite, it only allows frequencies below its set cutoff frequency. The filtered signal is passed onto an Operational Amplifier (op-amp) to amplify the signal. The attenuation of the signal in the body channel is about $-29dB$ (factor 0.035). This factor is calculated from Figures A.1 & A.2 which show measurements performed on the human body with both receiver and transmitter touching the human body using electrode-bracelets placed $1cm$ apart from each other on the same limb (arm). An example of the described circuit is provided in Figure B.3, which is the same circuit used for the prototype in this thesis.

The filtered signal is passed onto an op-amp, which is the same type as used in the transmitter, an OPA2863DR by Texas Instruments placed in a non-inverting amplifier configuration. A potentiometer is used as the ground resistor and the feedback resistor is fixed. The feedback resistor has a value of 580 $k\Omega$. The amplified signal is fed into an Analogue to Digital Converter (ADC). The ADC used is an 8-bit ADC of the type MAX11116AUT+T by Maxim Integrated. The eight bits are not fed parallel to the Field Programmable Gate Array (FPGA) but in series using Serial Peripheral Interface (SPI). A high-level overview of the receiver configuration is provided in Fig. 4.3.

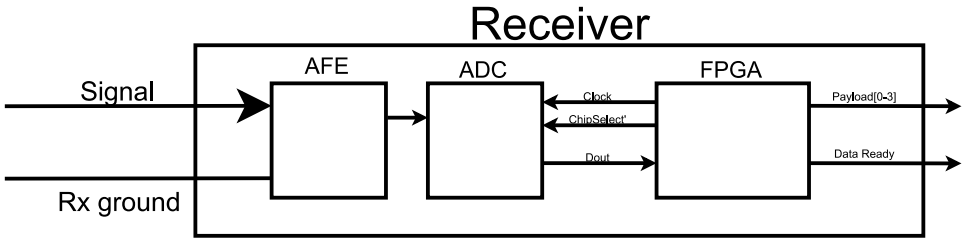

Figure 4.3: **High-level overview of the receiver**

4.4.2 Frequency Shift Chirp Spread Spectrum Modulation

The Field Programmable Gate Array (FPGA) that is the brains of the receiver, obtains the chirp signal in digital form from the Analogue to Digital Converter (ADC). The ADC is provided with a $6.25MHz$ clock signal from the receiving FPGA. The frequency of $6.25MHz$ used for the ADC could theoretically be higher in this setup as well but it was chosen to keep a lower value like this such that the system is more easily debugged on the oscilloscope used in the setup. The oscilloscope is a 4 channel Rigol

DS1104-Z-plus with a bandwidth of 100MHz and a sampling rate of 1Gsa/s.

Every sample period, the Chip-Select signal is pulled low by the FPGA and one 8-bit readout will be transmitted to the FPGA by the ADC. The readout is taken by the ADC when the Chip-Select is pulled down. The ADC used in the prototype is the Maxim Integrated MAX11116 with an Serial Peripheral Interface (SPI) communication link. The receiver's logic is run on a Nexys2 FPGA just like the transmitter. The output will be received payload and a flag to indicate when the payload is presented.

The process of dechirping in this prototype is described here, but the implementation (in Very-high-speed Hardware Description Language (VHDL)) is provided in Chapter 5. First, the FPGA samples the analogue signal at a sampling rate set to make sure, given the bandwidth, that 128 samples are taken for every chirp. The sampling rate depends on the spreading factor and bandwidth. An amount of 128 samples is chosen since the Fast Fourier Transform (FFT) -cores used in the FPGA only take arrays with lengths that have a power of 2. Taking only 64 samples would be under-sampling (Nyquist) and taking more samples (256) would create a buffer that takes too long for the FFT -core in VHDL to process for the current sampling rate. A visualisation of those 128 samples, taken of a chirp with symbol value 0, is provided in Fig. 4.4. From this visualisation, one can conclude that per period, more than two samples are taken at any time and hence, the Nyquist sampling theorem is met.

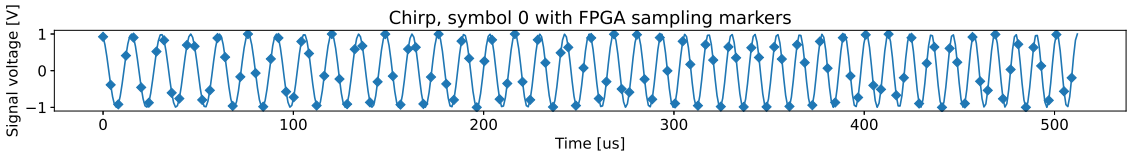

Figure 4.4: **Chirp with symbol value 0, showing the 128 ADC/FPGA sampling points**

The 128 samples taken, are, as can be seen in Fig. 4.4, real valued and not complex. However, (Frequency Shift) Chirp Spread Spectrum Modulation (FSCSSM) is based on, as explained in section 5, complex signals because FSCSSM was intended for Radio Frequency (RF) communication with In-Phase and Quadrature signals. To obtain the analytical and complex signal that is normally obtained with IQ signals, a Hilbert transform is applied to the 128 samples taken. It will be later mentioned that from those 128 samples, only 16 samples are effectively used. The number 16 is based on the Spreading Factor, which is set to 4 in this work. A spreading factor of four indicates that the chirp is split into $2^4 = 16$ chips as mentioned in the theory.

Applying the Hilbert transform to only those 16 samples would be beneficial in terms of resources, but the Hilbert transform will be incorrect since the true signal is under-sampled in that case. For that reason, the sampling rate should meet the Nyquist sampling theorem and 128 samples are chosen here to meet the Nyquist Sampling theorem $F_{sample} \geq 2 * (F_{centre} + \frac{Bandwidth}{2})$. From those 128 complex values, according to the dechirping process, 16 samples, equally spaced, are taken. One sample per chip. Those are multiplied with the down-chirp. The down-chirp is the complex conjugate of an up-chirp. The up-chirp is a chirp with a symbol value of 0. From those 16 down-chirp-multiplied values, the FFT is taken and its absolute value yields 16 frequencies and the magnitude of those 16 frequencies indicates the occurrence of that frequency. The frequency with the most occurrences is the value of the chirp.

The calculation of the chirp value is performed after collecting each single sample, so 128 times per symbol. A preamble is used to locate where each chirp ends and begins. Every time the calculation of the chirp value happens, the system (during the preamble phase) assumes that a single sample is the closing sample of the chirp (the 128^{th} sample). The last 128 samples have been stored, including the last sample mentioned here, and those are used to calculate the chirp value. That chirp value is stored in a buffer with the size of n times 128. Once, 128 calculations are spaced apart, the buffer matches the preamble pattern, and the system assumes that it has synced with the preamble. A flag can be triggered

for every 128 samples for as long as the payload is transmitted. The length of the payload is indicated by the first chirp after the payload. The length equals the value of that specified chirp, plus 1. Since a chirp can take up a value of 0 to 15, a value of 1 is added to indicate the length since a length of 0 is never to be expected and the throughput is maximized to a payload length of 16.

Not only is the maximum frequency of the system limited to the clock frequency of the FPGA but a custom clock divider cannot create all frequencies below the main clock frequency either. This is because, with a clock period of 20ns (frequency of 50MHz), the frequency of the clock divider should be a multiple of 20ns. For this reason, the sampling period in the receiver can be only a multiple of 20 ns. Since the sampling frequency has a direct relation with the bandwidth, only a selection of bandwidths can be applied. The bandwidth has a direct effect on the maximum centre frequency that can be applied, in combination with the spreading factor. For these evaluations, a spreading factor of 4 is set.

Due to the system having to take 128 samples into a Hilbert Transform, putting a sample in every clock cycle with a clock frequency of 50MHz (20ns), a new sample from the signal can be taken only after every 128 clock cycles ($2.56\mu s$).

$$\frac{1}{F_{sample}} \geq \frac{N_{FFT}}{F_{clock}} \Rightarrow F_{sample} \leq \frac{F_{clock}}{N_{FFT}} = \frac{128}{50,000,000} = 390625Hz \tag{4.1}$$

In eq. 4.1 it is determined that using this FPGA with 128 sample points, the sampling frequency of the receiver can be no more than 390.625kHz. The 128 sample points are the number of samples for a complete symbol (chirp), which is determined in section 3.3, and so the amount of samples per chip is calculated by $\frac{N}{2^{SF}}$. Given the amount of samples per chip and the period of one chip in eq. 3.7, there is a ratio between the Bandwidth and the sampling rate given in eq. 4.2.

$$\frac{F_{sample}}{Bandwidth} = \frac{N_{FFT}}{2^{SF}} \tag{4.2}$$

Combining equations 4.1 and 4.2 gives a maximum bandwidth for this system in eq. 4.3.

$$Bandwidth \leq \frac{2^{SF} \times F_{clock}}{N_{FFT}^2} = \frac{16 * 50,000,000}{128^2} = 48,828.125Hz \tag{4.3}$$

Since a Hilbert transform is to be applied to obtain an analytical signal, the sampling rate should comply with Nyquist. To comply with the Nyquist sampling theorem, the sampling rate F_{sample} should be at least twice the maximum frequency in the system. The maximum frequency is the centre frequency plus halve the bandwidth (eq. 4.4).

$$F_{sample} \geq 2 \times (F_{centre} + \frac{Bandwidth}{2}) \Rightarrow F_{centre} \leq \frac{F_{sample} - Bandwidth}{2} \tag{4.4}$$

Unfortunately, during this phase and before improvements, miscalculations took place which led to lowering the maximum centre frequency by the amount of the bandwidth. Doing so yields eq. 4.5. Evaluations have been performed with these lower maximum centre frequencies but can now also be performed with centre frequencies that indirectly comply with the Nyquist sampling theorem.

$$F_{centre} \leq \frac{F_{sample} - Bandwidth}{2} - Bandwidth \tag{4.5}$$

The combination of equations 4.1, 4.2, 4.3 and 4.5 provide a list of bandwidths that can be tested in this prototype with the given maximum centre frequency. One last requirement for options in the list is that the sampling frequency must be a multiple of 40ns, which is twice the clock period of the FPGA. This is true since the clock divider can change the value of the new clock only at every rising edge of the main clock. The list of frequency and bandwidth settings provided by these requirements is given in Table 4.1. The list is provided by iterating over all possible bandwidths and can be extended by decreasing the bandwidth step size. Lower bandwidths can be used as well and the list could be extended to way lower frequencies, which go beyond the purpose of these tests.

Bandwidth [Hz]	Maximum centre frequency [Hz]	Symbol duration [μs]	Sampling frequency [Hz]
39,062.5	97,656.25	409.6	312,500
31,250	78,125	512	250,000
25,000	62,500	640	200,000
15,625	39,062.5	1,024	125,000
12,500	31,250	1,280	100,000

Table 4.1: **Frequency settings used in the evaluations**

Chapter 5

Frequency Shift Chirp Spread Spectrum Modulation in Body Coupled Communication

A full model of the prototype is elaborated on in the previous chapter, Chapter 4. The chirps in the prototype are transmitted and received by a Field Programmable Gate Array (FPGA) since such a device can (easily) achieve processing speeds required for sampling at micro-second levels. In this chapter, the Very-high-speed Hardware Description Language (VHDL) design (implementation) of the transmitter and receiver are elaborated on. For both the transmitter and receiver, this chapter will explain that processing is not only taking part on the FPGA but on a computer as well and it will explain why that is.

5.1 Transmitter

The transmitter will convert symbols of a given value into analogue chirps which in turn are coupled to the human body. A packet (message) contains a preamble (multiple symbols), a delimiter, a length symbol and the payload symbols. All the symbols may be symbols with different symbol values so their chirps will have different characteristics. For ease of programming and ease of varying parameters, the chirps are prepared in Python.

A list of the whole message in analogue chirp form is provided sample by sample given a sampling frequency $F_{sample_{Tx}}$. Each value in the list corresponds to the voltage created by the Digital to Analogue Converter (DAC) at a given sample index. A list of frequencies is composed given the bandwidth and centre frequency and the number of samples calculated from the sampling frequency. Per chirp, the list of frequencies is cyclic-shifted such that the frequency shift is indicating the symbol value according to the theory for (Frequency Shift) Chirp Spread Spectrum Modulation (FSCSSM). Using the shifted list of frequencies, a sinusoidal wave is created. The wave is formed by iterating over each frequency in the list and per iteration calculating the cumulative sum of all frequencies, up to the current frequency, divided by the total amount of frequencies. In other words, the list with sampled and cyclic shifted frequencies is converted to a list of phases. A piece of pseudo-code is shown to provide a more visual explanation of what is used to obtain the list of phases and the chirp.

```
1    frequencies = {shift frequency to frequency B, frequency A to shift frequency}
2    phases = cumulative sum of frequencies
3    chirp = sine(2π * phases)
```

The list of samples is formatted into a list. The whole list can be pasted in the Very-high-speed Hardware Description Language (VHDL) design for the transmitter. The transmitter makes use of a virtual clock component (clock divider) to output a new sample of the list at the sampling rate.

The Field Programmable Gate Array (FPGA) clock frequency is 50MHz in this prototype. For a sampling frequency of 2.5MHz, every 10^{th} rising edge of the FPGA clock, the virtual clock changes state from 0 to 1 or 1 to 0. With a sampling frequency of 2.5MHz, a centre frequency of 78125Hz and a bandwidth of 31250Hz, one symbol has 1280 samples. The list will be as long as 1280 samples times the amount of symbols to be transmitted. In the prototype, the message "m" is sent which is 0x6d in hexadecimal form and divided over two symbols of each 4 bits, this would be a 6 (0b0110) and a 13 (0b1101). The preamble chosen is 0,4,8,12,15 in their binary form of 4 bits each. These values have been chosen since each of them is different and every bit is used at least once. Doing so, a clear distinction between the sent symbols is found but there is a recognizable pattern. Using the same symbol, for example, 0, could lead to the same positive false flags repeated which is not desired. The preamble is separated with the delimiter of value zero followed by the length of the message which is 2 (0b0010) in this case. The redundancy of the preamble is chosen by the receiver, but the transmitter sends each symbol from the length and payload trice for triple modular redundancy. The total amount of symbols is $5+1+3+3\times2 = 15$. The list will have a size of 19200 samples in the prior mentioned settings.

Per the sample transmitted, each bit is taken as a single output of the FPGA and each output is wired to the DAC. The DAC builds the analogue value from those bits. For each sample, ten bits have been used to compose the value since that is the amount that the DAC can take at once.

5.2 Receiver

The receiver is a bit more complex compared to the transmitter when it comes to Very-high-speed Hardware Description Language (VHDL) Design. Yet, a part is still analyzed in Python in the end due to ease of use and limited resources available on the Field Programmable Gate Array (FPGA).
At the sample rate $F_{sample_{Rx}}$, the receiver is sampling the analogue real-valued received signal. The sampling rate in the receiver is determined using a virtual clock designed in VHDL. The virtual clock is, just like the one in the transmitter, a clock divider and works the same.

The Analogue to Digital Converter (ADC) is making use of Serial Peripheral Interface (SPI) and for that reason another sampling module is designed in VHDL to provide a virtual clock between the ADC and collect the SPI data. The sampled data is stored in a First-in-First-out (FIFO) buffer with a size of 128 samples. The buffer is another component in VHDL. The buffer is used as input for the Hilbert transform. The Hilbert transform component makes use of a pre-designed Fast Fourier Transform (FFT) and Inverse Fast Fourier Transform (IFFT) module provided by the Xilinx CORE Generator of which the settings are provided in 5.1. The designed component for the Hilbert transform takes the 128 samples into the FFT component sample by sample at the rate of the system clock (50MHz) and repeats this process of taking 128 samples at the rate of the designed virtual clock. Because the 128 samples are taken into the FFT quicker than the sampling period, the FFT is idled for a given amount of clock cycles to match the sampling period. The Hilbert transform takes the FFT of N samples, sets the 2^{nd} half of the FFT output to zero and the whole is them subjected to an IFFT. The IFFT component is, just like the FFT component, built using the Xilinx CORE Generator.

Settings for the IFFT component are similar except for the following items:

- Precision Options: data width = 18, factor width = 12
- Input Data Timing: No offset

The real-valued signal is now sampled and buffered into a buffer the size of one chirp. The buffer is converted into an analytical signal having both the real and complex component. Using the analytical signal, the mathematics that apply to (Frequency Shift) Chirp Spread Spectrum Modulation (FSCSSM) can be applied. To apply the maths, the analytical signal is under-sampled such that from the 128 samples, only 16 are taken equally spaced apart. The selection is right away applied in the Hilbert

Setting	Value
Channels	1
Transform length	128
Target clock frequency	50MHz
Implementation option	Pipelined, Streaming I/O
Data format	Fixed point
Precision options	Data width:9; factor width: 12;
Scaling options	Unscaled
Rounding modes	Truncation
Optional pins	CE
Output ordering	Natural order (no cyclic prefix insertion)
Input data timing	3 Clock cycle offset
Number of stages using Block RAM	0
Reordered buffer	Distributed RAM
Complex multipliers	Use 3-multiplier structure
Butterfly Arithmetic	Use CLB logic

Table 5.1: **The settings for the pre-designed FFT component, using the Xilinx CORE Generator**

component.
The 16 samples that have been selected are forwarded into the dechirper. The dechirper performs a multiplication with the downchirp (also undersampled to 16 samples) using the downchirp component. The downchirp samples are pre-calculated in Python and each one of them are placed in a VHDL function format with its name corresponding to the sample index. The down-chirp multiplications are all binary multiplications, the Python script helps to quickly build the correct-valued functions for the down-chirp multiplications. The down-chirped samples are submitted to another FFT but this FFT is not a pre-designed FFT component. This component, however, is a custom VHDL design. Once again a custom built Python script creates the VHDL design for the N-Point FFT.

The FFT design can be scaled using this Python script, which was not required in the end but still useful to obtain a better understanding of how an FFT is actually performed. It was chosen to use a custom built FFT since the pre-defined would use resources that where no longer available. Those resources were mostly used by the Hilbert transform. The absolute values of the dechirped signal are compared to each-other and the index at which the value is the highest is assumed to be the symbol value of the chirp. To obtain the absolute values of the dechirped signal, they are multiplied by themselves using a pre-designed multiplier from the Xilinx CORE Generator. Settings for the CORE Generator, just like those for the FFT and IFFT are listed here.

- Multiplier type: parallel Multiplier
- Input Port A and B data type: signed
- Input Port A and B Width: 11
- Multiplier Construction: Use LUTs
- Pipeline Stages: 0

Now that the signal is dechirped, a synchronisation component stores a large buffer of past dechirped values. Note that at each new sample taken from the analogue signal, the whole process is repeated,

so only once every 128 samples the actual chirp value is obtained at the correct moment in time. That moment in time is where the sample matches with the end of the chirp. To find that point, the synchronisation component looks back in time where, 128 samples apart, the received symbol values do match those of the expected preamble. Using the synchronisation point, a message-decomposer component processes received data. The output of the dechirper, synchronisation component and message decomposer component are forwarded to physical outputs of the FPGA such that a logic-analyzer can pickup those outputs and store them in a digital format. A Python script can analyze the stored data from a Comma Separated Values (CSV) file.

Chapter 6

Evaluation

The goals of this thesis are to provide a prototype of Body Coupled Communication (BCC) with the use of (Frequency Shift) Chirp Spread Spectrum Modulation (FSCSSM) and measure the effects of changing parameters from this prototype. The effects of parameter changes should provide an insight into the performance of the combination of BCC and FSCSSM. The performance indication could be used as a guide for further designing this system and/or determining its benefits over other systems.

Parameters that could influence the system's performance are transmitter gain, body composition, distance, electrode dimensions, electrode inter-distances, receiver gain, frequency, bandwidth, spreading factor and noise levels. All contributions of these parameters should, at some level, be looked into and for each of those, one or more tests are performed to do so.

6.1 Frequency, bandwidth & data rate

Since the human body is frequency selective and the modulation technique is all about changing frequency, evaluating the effect of changing the centre frequencies is one of the reasonable things to do.

6.1.1 (Centre) Frequency

In this system, the centre frequency has no direct effect on the data rate. This conclusion can be drawn by taking a look at eq. 3.8 which is the time of a single chirp, for which the centre frequency is no parameter. To show that this parameter does not affect the overall data rate, a plot is created with settings applied to the model in this thesis. The plot is shown in Fig. 6.1 and also the parameter bandwidth is included to show that the bandwidth does influence the data rate. As expected from eq. 3.8, when the bandwidth increases, the data rate does so too as is shown in Fig. 6.1, which is a simulation.

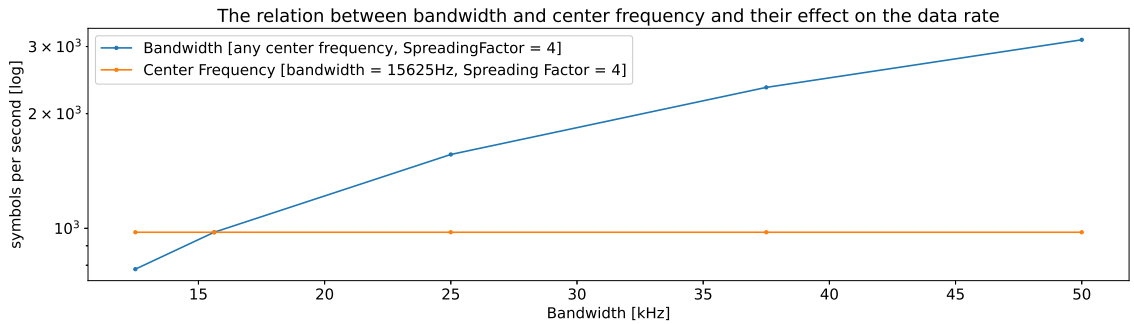

Figure 6.1: **Relation between data rate and both the centre frequency and bandwidth**

This is a simulation, however, and no real-world experiment. In this simulation (Fig. 6.1), the effect of the centre frequency is not measured. An evaluation with the following parameters was performed, to obtain the actual effect of changing the centre frequency.

- Input voltage: 3V
- Bandwidth: 12500Hz
- Distance between Transmitter (Tx) and Receiver (Rx): 5cm
- Inter-distance: 1cm
- Spreading Factor: 4

In this evaluation, of which the result is shown in Fig. 6.2, multiple centre frequencies have been evaluated with a fixed bandwidth. For each evaluation, the receiver gain was adjusted to the minimum gain for which the receiver can receive and decode the messages with an error of 0%.

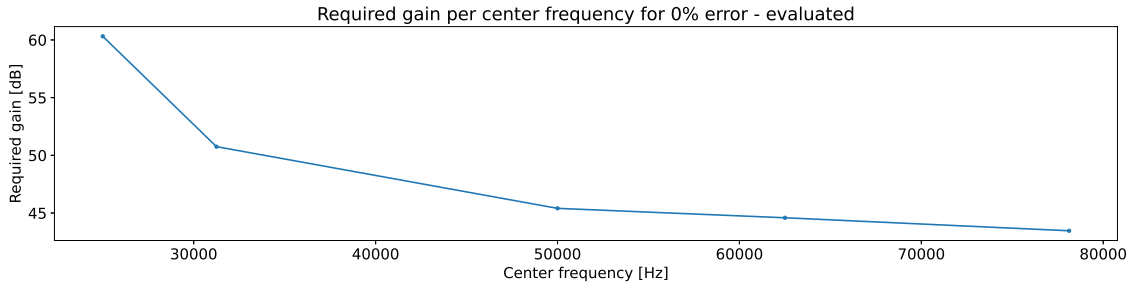

Figure 6.2: **Relation between the received signal strength and centre frequency**

From the evaluation it becomes clear that a higher frequency requires less gain. Less gain is required since the signal is propagating through the body better and more signal strength is received at the receiver. This conclusion is not a direct cause of the use of chirps. However, it does suggest that using a higher centre frequency in the chirp results in a better chance of decoding the message successfully. Using Signal-to-Noise Ratio (SNR), this conclusion is looked into further. While the gain is system-specific, SNR is not.

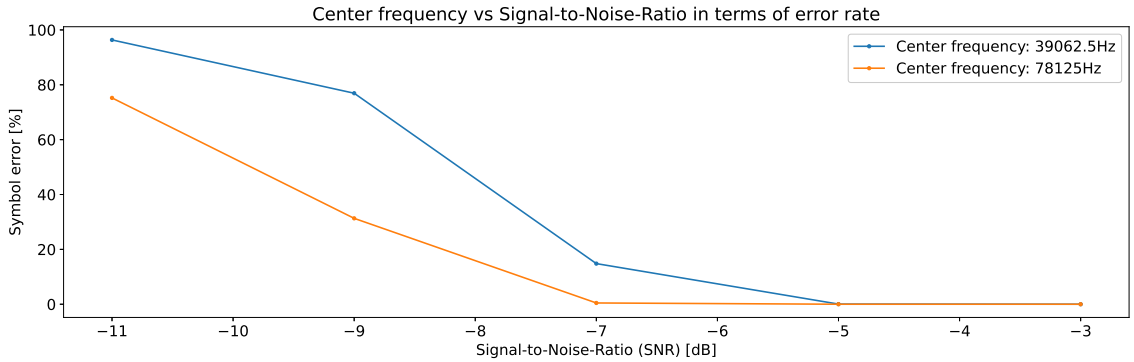

Figure 6.3: **Relation between the Signal-to-Noise-Ratio and the centre frequency**

In Fig. 6.3 the relation between the centre frequency and the SNR is depicted. This figure backs up the conclusion that with a higher centre frequency, the signal propagates through the body better compared to lower centre frequencies. The highest centre frequency in Fig. 6.3 (orange line) can achieve a 100% reception rate with worse SNR compared to a lower centre frequency (blue line).

From these two evaluations, the suggestion is presented that higher (centre) frequency performs better. That suggestion must be provided with a different perspective because, as is concluded from prior research, a higher frequency also means more probability of signal leakage. A trade-off between the amount of signal allowed to leak and the level of propagation is present.

6.1.2 Bandwidth

An important measure of a communications system is the data rate. Data rate is not the key in this thesis but privacy and reliability are. However, since the data rate is bandwidth-dependent and different bandwidths have different frequency footprints, the data rate is indirectly evaluated as well. For all bandwidths, the required receiver gains are set to achieve a 100 percent reception rate.

- Input voltage: 3V
- Centre frequency: 31250Hz
- Distance between Transmitter (Tx) and Receiver (Rx): 5cm
- Inter-distance: 1cm
- Spreading Factor: 4

The expectation is that, when noise is limited, the received signal strength will be affected only with a very small factor by the bandwidth. More bandwidth should allow more spreading of the signal compared to noise but a downside is visible from the centre frequency analysis. Increasing the bandwidth will take up a broader frequency spectrum and the distance from the centre frequency is increased using a broader bandwidth. At low frequencies, which are used in the prototype built for this thesis, the part of the bandwidth below the centre frequency will have fewer propagation benefits compared to the frequencies in the bandwidth above the centre frequency. That note means that not the whole frequency range in the bandwidth will have the same ease of propagating through the channel.

The effect of using different bandwidths is shown in Fig. 6.4. In this evaluation result, the effect of bandwidth, indeed, seems negligible. The differences between measurements are within less than 1 dB and are most likely due to measurement errors rather than the true effect of the bandwidth. The latter conclusion is drawn due to the differences not being linear over the bandwidth spectrum.

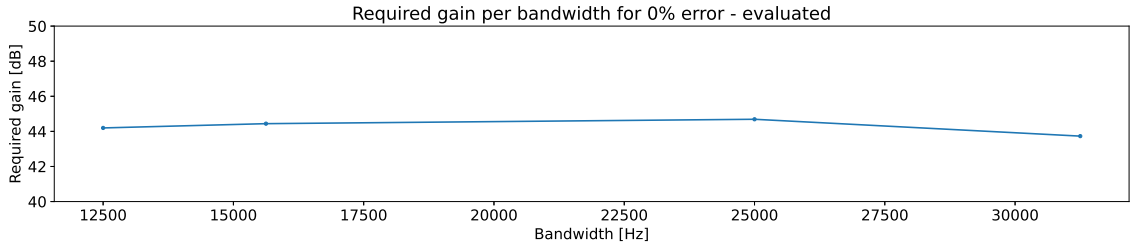

Figure 6.4: **Relation between the received signal strength and the chirp bandwidth**

These results are in line with the expectations found by Ahmed et al. in 2020([1]). In their work, the attenuation slope is gradually decreasing as the frequency increases. For low frequencies, the gain required in this prototype is large and the attenuation in the work of Ahmed et al. is very low. The slope to the next measured frequency is steep in this evaluation and in their work. For the higher frequencies evaluated these slopes are not as steep in either works. The effect of why higher frequencies are better in propagating is explained in [18]. Quoted from their work: "At lower frequencies, the

dielectric property of the skin is dominated by the outermost layer of the skin called stratum corneum (SC), which is composed of dead and flat skin cells" - "The effect of SC vanishes as frequency increases; this phenomenon is manifested by the decreasing skin impedance." [18].

6.2 Spreading factor

The two aspects that influence data rate and resistance to noise are the bandwidth and the spreading factor. Increasing the latter is beneficial as was shown in Fig. 3.13. Doing so, however, requires a large part of the receiver to be rewritten. In this work, this is not evaluated and the theory is used as the basis for motivating that a larger spreading factor should benefit reliability to noise.

6.3 Electrode inter-distances and dimensions

In various related works, the dimensions of electrodes and the distances between the two electrodes of a pair (inter-distance) are proven to affect the received signal strength. Both of these factors have been evaluated for this work and they are compared concerning Signal-to-Noise Ratio (SNR).

6.3.1 Inter Distance

As was described by eq. 3.2, the received signal strength is expected to be dependent on the inter-distance. An evaluation will be performed where the inter-distance on the transmitter is varied between 0.5cm and 3.5cm for the same variety of distances on the receiver inter-distance.

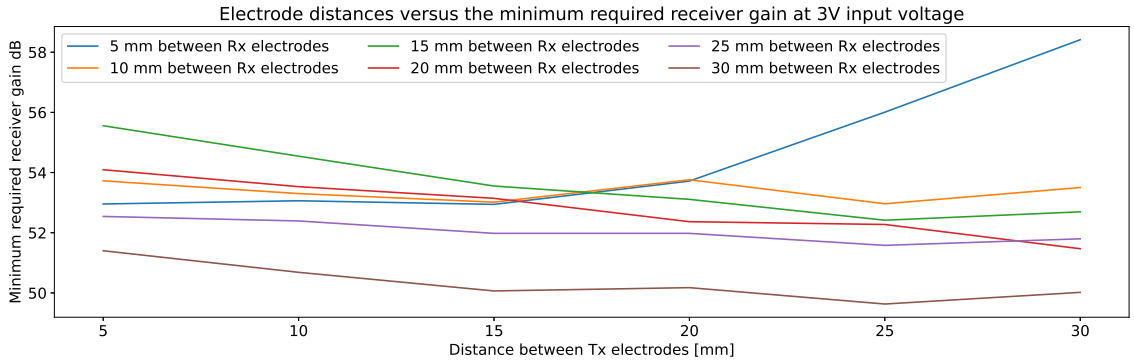

Figure 6.5: **Relation between the received signal strength and the inter-distance of electrodes**

From this graph, shown in Fig. 6.5, the effect of changing the inter-distances becomes clear. Except for inter distances of 5 and 10mm, the received signal strength increases for a greater inter-distance. The distances between the electrodes are nowhere near the wavelength, half of the wavelength or a quarter of the wavelength of the transmitted signal. This conclusion is important because it shows that the system behaves more like a capacitive coupled system the greater the distance between the two electrodes of one device, rather than a galvanic coupled system. Due to body impedance, the current flowing between the two plates becomes very limited the greater the distance. According to the formula of the electric field generated between two plates, found in eq. 3.1, the electric field generated should become smaller with greater distances. However, given prior research, it is also known that a capacitively coupled system has a stronger signal strength. Requiring less gain, as is shown in Fig. 6.5, for a greater inter-distance means that the signal strength received is stronger. Since the signal strength is becoming stronger, the conclusion is drawn that, to use a system that behaves like a waveguide, it's best to keep the inter-distances small. However, for 5 and 10mm the behavior seems unpredictable. An inter-distance of 15mm to 20mm is suggested as being optimal.

The 15mm to 20mm electrode inter-distance is suggested as being optimal not only due to the received signal strength but also because of practical reasons. Often, wearables are small so this system should

integrate easily. For medical applications devices are either implanted, for which dimensions matter, or they are worn on the body surface and are, thus, desired to be discrete.

Given the results in Fig. 6.5, the inter-distances 1, 2 and 3cm (or 10, 20 and 30mm respectively) are evaluated once more but not concerning the minimum required gain for a 100% reception rate, but for the symbol error rate per Signal-to-Noise Ratio (SNR).

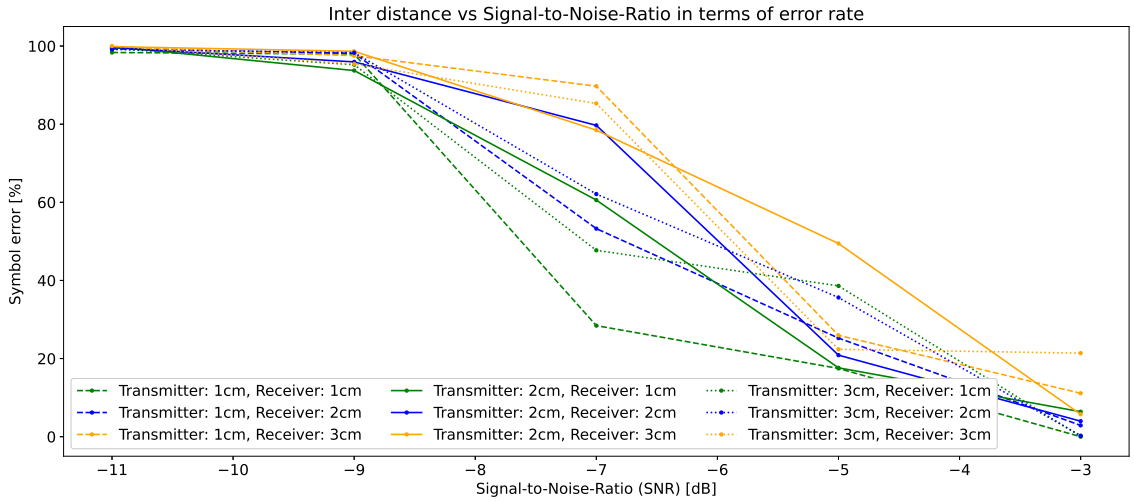

Figure 6.6: **Relation between the received signal error per SNR and the inter-distance of electrodes**

The results of the evaluation are depicted in Fig. 6.6. From these results, it can be concluded that the inter-distance of the receiver has the most influence on the system. The limited number of evaluation points in this experiment enforces the side note that conclusions drawn on this experiment are not strong. However, the receiver is best to be kept at a centimetre inter-distance rather than two and the transmitter is a little less of an influence but best to be kept around 1cm as well.

For both evaluations regarding the inter-distance, the system has been provided with the following parameters.

- Input voltage: 3V
- Centre frequency: 97656.5
- Bandwidth: 39062.5Hz
- Distance between Transmitter (Tx) and Receiver (Rx): 5cm
- Spreading Factor: 4

However strong these findings may be, both evaluations do not match the expectations found in related work. Arai et al. found in 2016 that increasing the inter-distance would increase the received voltage [2]. Differences might be related to either one or two factors. In their work, communication is established by touching an object which has the receiver. For this reason, the turning point might be occurring at greater inter-distances but this is not confirmed. Another difference between this and the research from Arai et al. is the orientation of the electrodes. Their electrodes are placed in series concerning the path of propagation while in this thesis, the electrodes are placed in parallel. The latter has not been evaluated in this thesis but might be an interesting evaluation for future work. For wearable applications or medical applications, the inter-distance is small in an ideal situation and has the least signal loss. From what it looks like, the work in [2] has the least loss at greater inter-distances but the difference with this work at the same distance for different orientations has not been compared.

6.3.2 Electrode dimensions

To verify the effect of electrode dimensions on the received signal strength, three different dimensions of electrode pairs are created and evaluated with a 5cm distance between the transmitter and receiver and 1cm inter-distance.

Three electrode dimensions are considered. In all evaluations, the electrode dimensions of the Transmitter (Tx) were set to the same dimensions of the Receiver (Rx). These dimensions were (15mmx20mm, 10mmx10mm, 5mmx5mm). The evaluation clearly shows that smaller electrode dimensions have a weaker received signal. For the largest electrode dimensions, the system achieved 0% error from -9dB Signal-to-Noise Ratio (SNR). A 0% error rate was not achieved for the smallest electrode dimensions and only at -3dB SNR for the electrode dimensions with 10mm x 10mm dimensions.

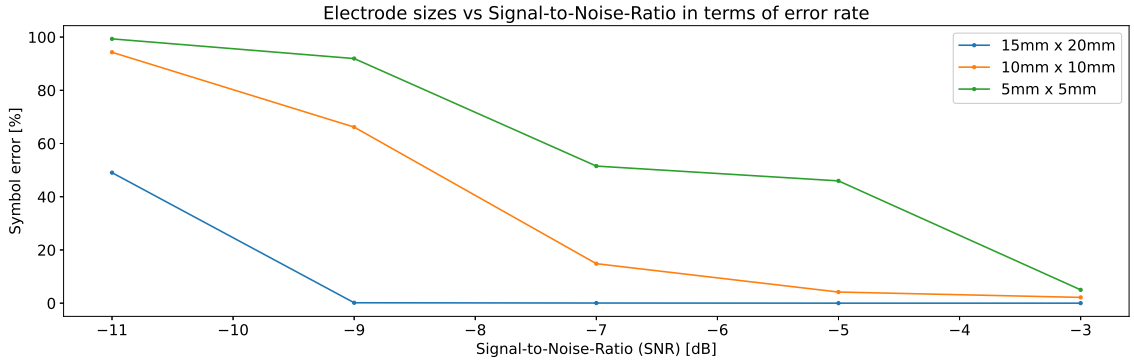

Figure 6.7: **Relation between the received signal error per SNR and the dimensions of electrodes**

These evaluations were performed with the output gain kept the same for each dimension, which might not be the best gain overall. This mention is provided since from these results, a statement that the smallest electrode dimensions cannot achieve a high SNR is not by definition true. The maximum achievable SNR for the smallest electrode dimensions was not evaluated.
In this evaluation, the following parameters were used in the system.

- Input voltage: 3V
- Centre frequency: 97656.5
- Bandwidth: 39062.5Hz
- Distance between Tx and Rx: 5cm
- Inter-distance: 1cm
- Spreading Factor: 4

While the inter-distance evaluations performed for this thesis were not directly in line with the results from related works, the effects of electrode dimensions were. In [2], larger dimensions had received bigger potential differences in voltage compared to smaller dimensions. This result was also found in this thesis and greater dimensions allowed for transmission with a signal of SNR -9dB without loss of data.

6.4 Amplifier and Receiver gain

The signal strength is determined not only by frequency and electrode configurations but also by the voltage at which the signal is coupled to the body (the input voltage). The relation between input voltage and gain required at the receiver is evaluated. Amplification at both ends requires power and the more amplification required at either end, the less power-efficient the system becomes. A less power-efficient

system is not desired since the modulation scheme (Frequency Shift) Chirp Spread Spectrum Modulation (FSCSSM) is considered very power-efficient. The power efficiency provided with this scheme in Body Coupled Communication (BCC) could allow for applications which rely on battery-less operation, such as implants.

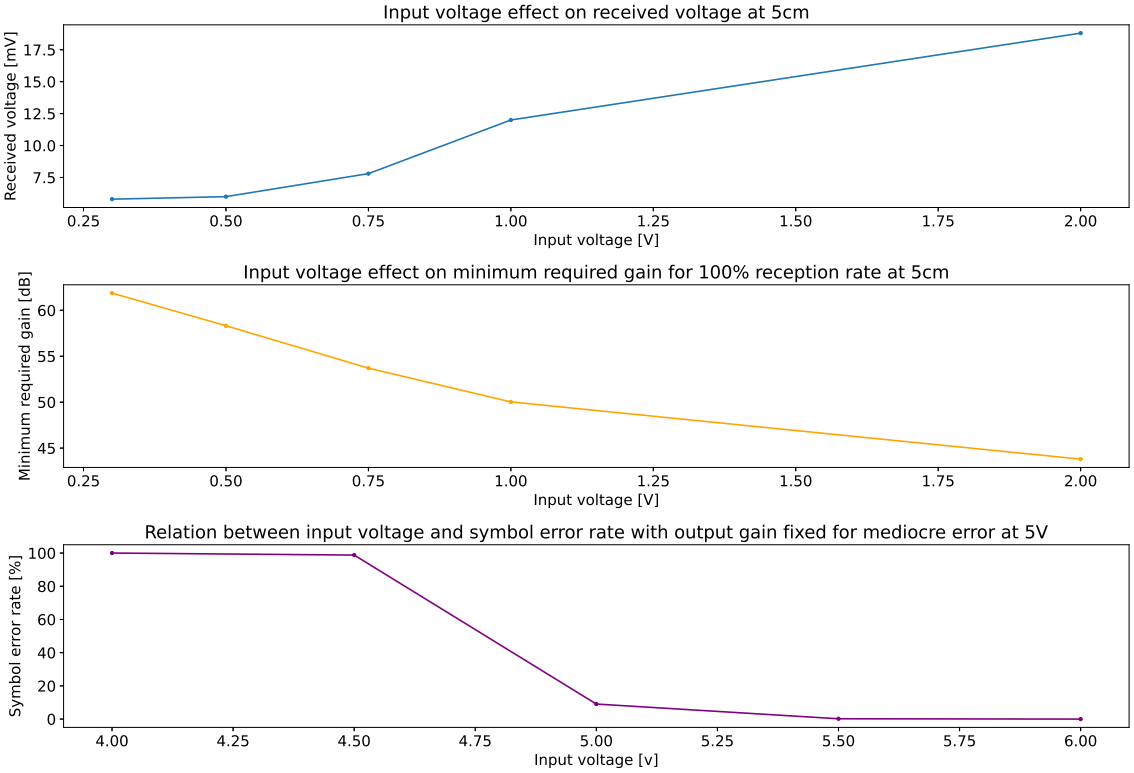

Figure 6.8: **Various effects of the input voltage**

The effect of input voltage and the effect of output voltage is visualized in Fig. 6.8 using three evaluations. The first evaluation shows how the received voltage is affected by changing the input voltage on the transmitter. From this evaluation, the received voltage is changed most between 0.5V and 1V from which the voltage gradually increases with a lesser slope. With that finding one can conclude that using more input voltage means using more power with lesser effect from after around 1V. A side note is that this does not have to be 1V exactly, since the effect is only tested at a few input voltages. The same effect, however, is found in terms of required gain. Between 0.25V and 1V the gain required in this system for a 100% reception rate has a steeper slope compared to the slope between 1V and 2V.

The last evaluation shows that the symbol error rate switches from about 100% to 0% within a window of 1V. When the error was set to be mediocre around 5V input voltage, the symbol error rate was found to be about 100% at 4.5V input voltage and about 0% around 5.5V input voltage.

These experiments were performed using the following system parameters:

- Bandwidth: 12500Hz
- Centre frequency: 31250Hz
- Distance: 5cm
- Inter-distance: 1cm

6.5 Transmission distance and body composition

Devices that make use of Body Coupled Communication (BCC) for communication with other devices in and around the body, can be placed at any location close to or (relatively) far away from each other at any undefined location. At any of the placed locations, these devices should be able to transceive messages without error. Even, as is evaluated in this thesis, the devices should be able to transceive to devices on another person's body who is touching the host body. Various related works have (successfully) tried to model the human body or even two human bodies touching in terms of BCC characteristics so best practices of where to place BCC devices are known. For medical applications, however, the most optimal spot for communications could be the worst spot to place a device for other reasons which might be more important. For these reasons, the desire is for the BCC system to be able to operate at each and any location. The prototype devices are placed at various distances from each other on the human body and spots having a different body composition. By finding weak spots or distances, the system can be evaluated for performance at those spots when the gain is tweaked. The desired result is having a system that can communicate without error with each and any device anywhere on the body or even in and around another person's body who is touching the host body.

In wireless communication, transmission distance is a factor in the received signal strength. For that reason, distance is evaluated in this work as well. A series of distances is evaluated on multiple persons. In this series, the distances are 5, 10, 20, 30, 40, 80, 100, 120 and 140cm. Because electrodes are placed on bands designed for the arms, the electrodes cannot be placed on parts of the body like the torso. The results are compared to the 5cm distance at which the gain is set such that the reception rate is expected to be 100%.

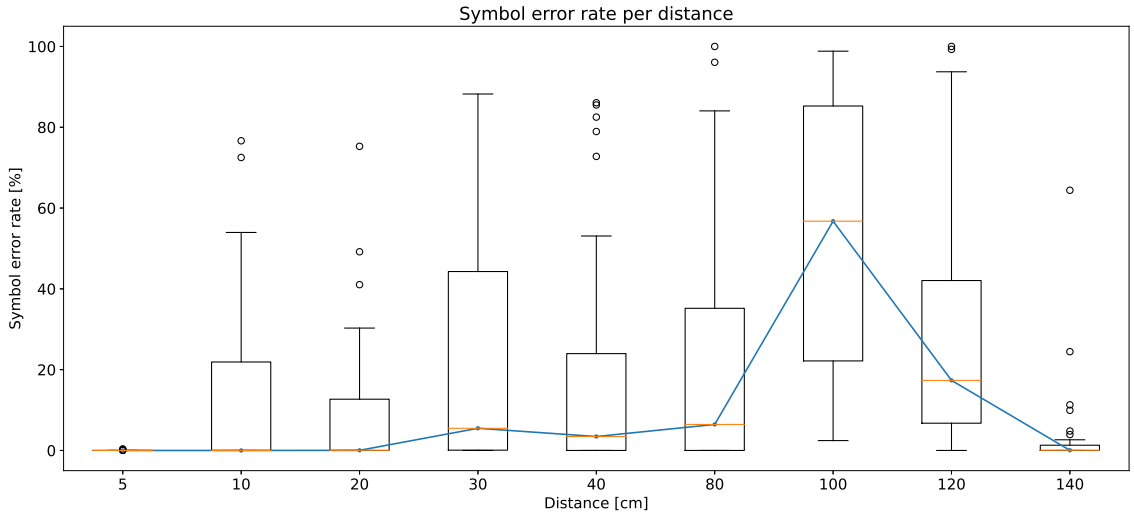

Figure 6.9: **Relation between the distance and symbol error rate**

The measurement results are depicted in Fig. 6.9, for all persons. Where a linear increase in error rate vs distance is expected, these results show otherwise. Even per distance, the results for various persons are very different. An explanation for this is found in body composition. For each person, the body composition is very different. Where 140cm is about always from one wrist to the other or at least one lower arm to the other lower arm, the median error between the same lower arm and the other lower arm is very similar. Given this finding, the distance is not found as the factor with the most impact on the error rate but the position at which electrodes are placed is. Muscle areas are found to have the worst conditions for BCC.

Applying the electrodes on positions not regarding distance but the body parts, the results are more in line with each other. This can be seen in the evaluation where body-to-body communication is evaluated. In Table 6.1 the error is graphically provided for various positions where the transmitter is placed on

one body and the receiver on another body. The two bodies (persons) are touching by holding hands.

Position	A_1 [%]	B_1 [%]	A_2 [%]	B_2 [%]
furthest wrist - furthest wrist	27.11	0.0	93.99	0.0
nearest shoulder - nearest shoulder	0.0	0.0	36.36	0.0
nearest wrist - furthest wrist	0.0	0.0	0.0	0.0
nearest wrist - nearest shoulder	0.0	0.0	11.69	0.0
nearest wrist - nearest wrist	0.0	0.0	0.81	0.0

Table 6.1: **Relation between the electrodes position and symbol error rate in body-to-body communication. (A_x = Symbol error rate threshold gain duo x, B_x = Symbol error rate normal gain duo x)**

While distance on a single body was not found to be a culprit, in body-to-body communication this factor starts to pose a problem as is found in Table 6.1, in the columns indicated by the letter "A". Also, the shoulder, where the muscle is found, is an example of being in a tough position to achieve communication with threshold settings as was concluded from the distance evaluation. Table 6.1 is accompanied by measurements at higher receiver gain to show that, even at worst conditions, communication is possible with an error rate of 0%. The columns with those results are indicated by the letter "B".

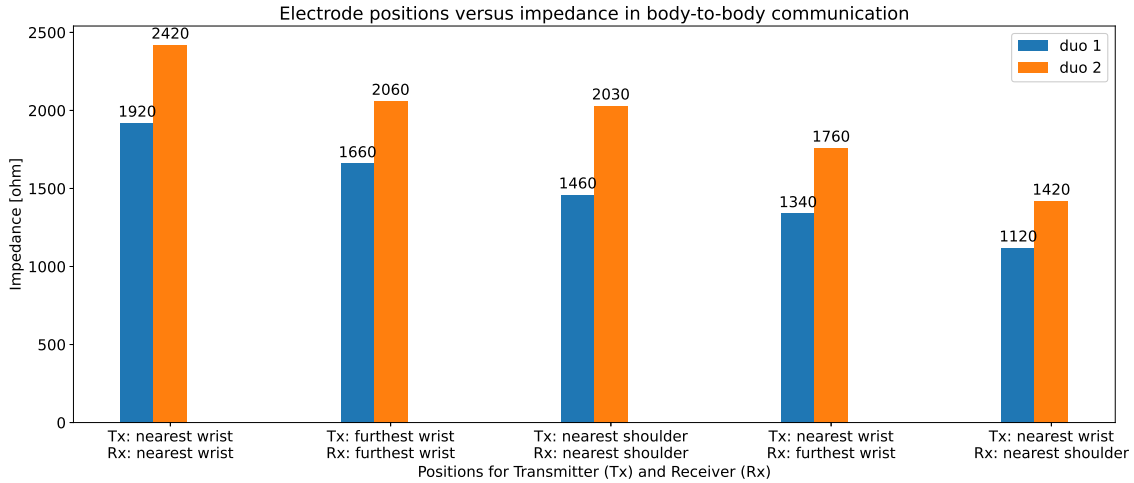

Figure 6.10: **Relation between the position and impedance of the electrodes in body-to-body communication**

An attempt was made to clarify the results using impedance. For the positions at which body-to-body evaluations were performed, the impedance is also being measured. The error rate occurring over distance can be related to the overall impedance that is the largest measured at the greatest distance. Shown in Fig. 6.10. The error rate related to body composition, however, is hard to clarify using these impedance measurements. While the conclusions on the matter regarding body composition from related works still hold, the evaluations performed in this work do not provide a quantified verification.

All the evaluations in this section were performed with the following system parameters, while the other factors were changed according to the measurement as mentioned.

- Input voltage: 2.6V
- Bandwidth: 12500Hz

- Centre Frequency: 31250Hz
- Inter-distance: 1cm
- Spreading factor: 4

By Ahmed et al. it was concluded that for a frequency of 10kHz, the signal is confined in the skin and fat layers while at higher frequencies (1MHz) the signal is limited to the surface of the body [1]. This same conclusion is found by Kibret et al. in [18] where they graphically show the influence on the impedance for all four layers of the human through which the signal can propagate (skin, muscle, fat and bones). They find that fat is about constant in terms of impedance and the other three layers decrease in impedance over frequency. However, while the impedance of skin drops by a factor of about 10 from 20kHz to 1MHz, the other layers do not drop in terms of impedance that much which explains the findings of Ahmed et al.

Muscle and fat have relatively large impedances and since, at low frequencies as used in this thesis, they play a role in propagating the signal, body parts with lots of fat and or muscle have worse results as was found in this thesis. Moreover, thick skin at low frequencies can affect the signal negatively since the skin, especially at low frequencies, has a very high impedance.

In this evaluation, it can be concluded that body position (composition) is more important (at lower frequencies) than distance when considering single-body communication. In [22] this can be seen as well. While their work might not conclude directly the relation between distance and body composition, their measurements which were performed on the upper arm location where muscle and fat are more in play have a lower attenuation and not a linear decrease compared to the difference between the other two locations where they measured. With the conclusion of this thesis about body composition being more important for the lower frequencies, their results might also be affected by this phenomenon without them being aware of that.

6.6 Noise levels

One of the main aspects of this research is reliability. Reliability is the most important argument for using (Frequency Shift) Chirp Spread Spectrum Modulation (FSCSSM) in this work and comparing its effect to other modulation schemes in Body Coupled Communication (BCC). Specifically, the reliability concerning noise is of interest. The body is a noisy antenna and not just prone to picking up signals meant for BCC but, for example, 50Hz is a very present signal. Using a bandpass filter already reduces much of the noise but FSCSSM is known for being able to go below the noise floor. To measure the effect of noise on the system, the transmitter signal is created with various levels of Signal-to-Noise Ratio (SNR), starting at 0dB and going down to -16 dB. Received signal strength is hard to measure but the percentage of messages that can be decoded is not.

For each SNR in the range of 0dB to -16dB, a record of 4 to 10 seconds is taken and the amount of packages that could not be decoded is the error level as a measure of how well this system performs in terms of stability and reliability.

- Input voltage: 3V
- Bandwidth: 12500Hz and 31250Hz
- Centre frequency: 31250Hz for BW=12500Hz, 78125Hz for BW=31250Hz
- Distance between Transmitter (Tx) and Receiver (Rx): 5cm
- Inter-distance: 1cm
- Spreading Factor: 4
- Receiver gain: most optimal for each SNR

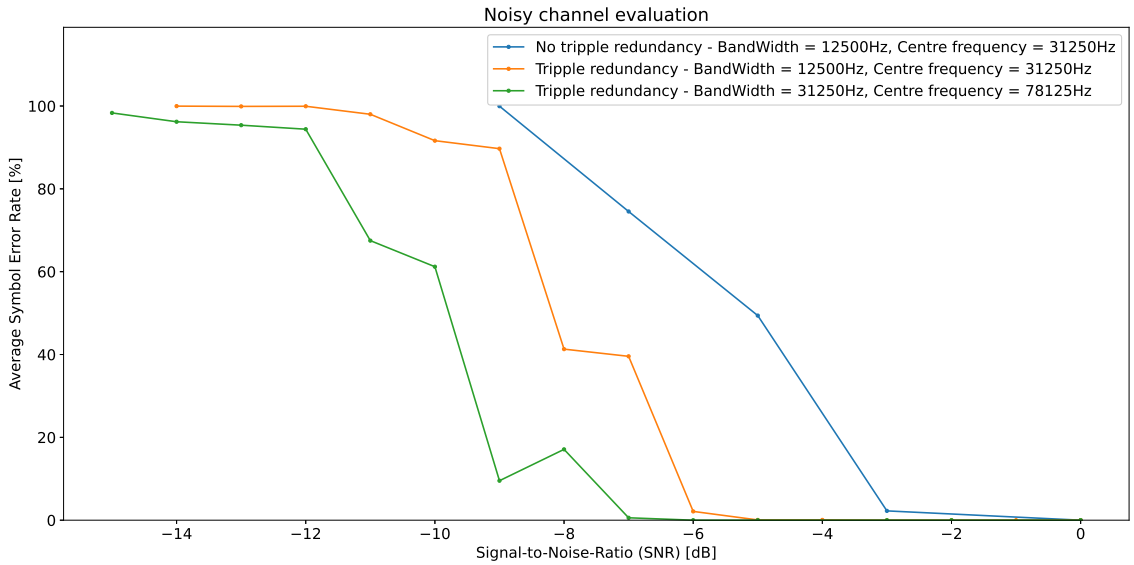

Figure 6.11: **Relation between the SNR and error rate**

In Fig. 6.11, three evaluations are combined for comparison. The effect of SNR is evaluated for two different bandwidths and also the difference between transmission with triple modular redundancy and transmission without triple modular redundancy is evaluated. The worst result is found when using the lowest bandwidth possible and using no triple modular redundancy. Yet, even this modulation achieves communication with an SNR below the noise floor. For the same bandwidth and centre frequency, triple modular redundancy is applied to allow for a bit more redundancy, yielding communication with about 0% error when having an SNR of -6dB. When increasing the bandwidth to 31250Hz, about 0% error is achieved during communications with an SNR of -7dB. During all evaluations, the best SNR achieved was -9dB whilst having a 100% packet reception rate. This result is seen in Fig. 6.7. The centre frequency for this result is at 97656.5Hz, the bandwidth at 39062.5Hz and the input voltage was 3V. Using these parameters, a data rate of 2.4 kilo-symbols per second is achieved at a SNR of -9dB without error.

These noise levels were not found in any other related work that is making use of Galvanic Coupling (GC) and is keeping an eye on privacy. Yet, it must be noted that data rate is a trade-off in which privacy is often discarded too easily.

6.7 Analytical signal

In the theory, model and implementation chapters, it is explained that the receiver takes 128 samples per symbol and performs a Hilbert transform on those to obtain an analytical signal of the received, real, signal. According to the maths provided in Chapter 3, a complex signal has to be undersampled with the frequency of $\frac{1}{bandwidth}$. The samples are to be multiplied with a down chirp (complex conjugate of a chirp with symbol value 0) in its complex form. From that multiplication, the Discrete Fourier Transform (DFT) will provide the symbol value of the chirp signal. Because some remarks had been found during the dechirping process simulations, the absence of complex signals is evaluated as well.

These evaluations are pure simulation results of processing a signal in one of the following three methods:

1. Obtain the analytical signal of the received signal and multiply it with the down chirp in its complex form.
2. Multiply the received signal in its non-complex form with the down chirp in its complex form.
3. Multiply both the received signal and the down chirp in their non-complex form with each other.

When a Hilbert transform is applied in the first method, the analytical signal is then undersampled and multiplied with the down chirp in its complex form. In the other two methods, the received signal is not subjected to a Hilbert transform and it is directly undersampled before multiplication.

This evaluation is important since not having to perform a Hilbert transform could spare a lot of resources in hardware. Not having to use a Hilbert transform could lead to a more power-efficient decoding process, could allow for a higher spreading factor and could even make this process be implementable on micro-controllers rather than specific hardware such as an Field Programmable Gate Array (FPGA).

6.7.1 Method 1

Method 1 is the method used throughout this thesis. This method requires a Hilbert transform.

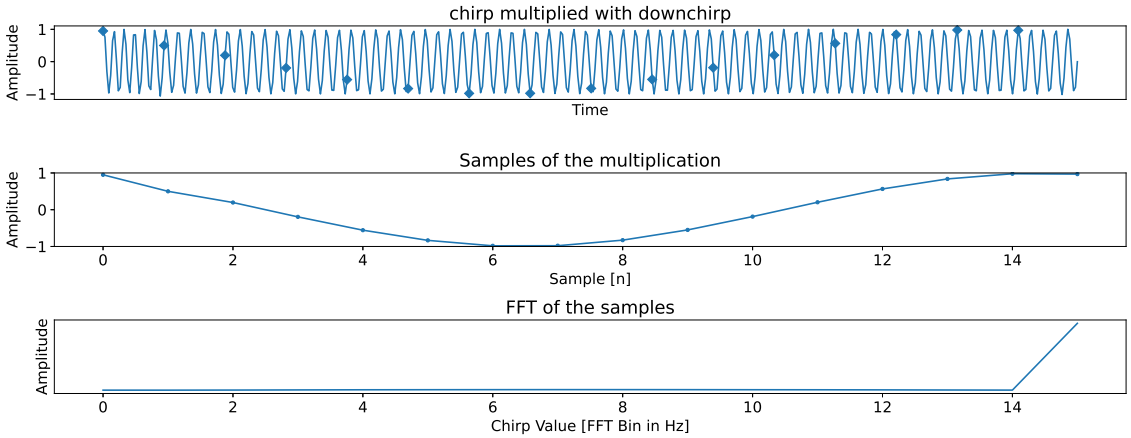

Figure 6.12: **Dechirp process method 1**

In Fig. 6.12 the process is visualized using method 1. As is expected, the frequency response is flat and shows a peak on bin 15, which is the symbol value of the chirp used in this simulation. The other bins are valued at zero. This result is as expected and can be used as a comparison for the other two methods.

6.7.2 Method 2

Method 2 is the method that takes the received signal as is and undersampled. That undersampled signal is multiplied by the down chirp. The results are visualized in Fig. 6.13.
The frequency response still shows a peak at bin 15, which is the transmitted symbol in the simulation. However, there is another frequency component visible in the multiplication waveform of Fig. 6.13, showing that this method is not as ideal as method 1. However, the important conclusion here is that the received signal can be taken as a real-valued signal without the need for a Hilbert transform. The signal, however, will be less resilient to noise. That can be overcome by increasing the spreading factor which is easier to do when resources are not used for a Hilbert transform. Increasing the Spreading Factor requires fewer resources than the Hilbert transform would.

6.7.3 Method 3

In method 3, both the received signal and the down chirp are in their non-complex form and multiplied together. The result is visualized in Fig. 6.14. According to the frequency spectrum, there is no clear distinction between bin 1, bin 3, bin 13 and bin 15. Due to that ambiguity, the system could not detect which symbol value was assigned to the chirp and the payload would be lost.

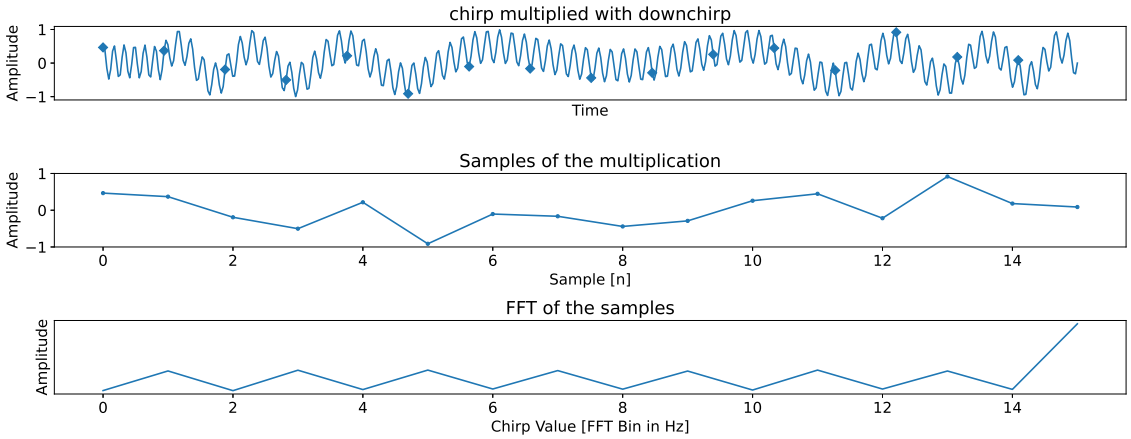

Figure 6.13: **Dechirp process method 2**

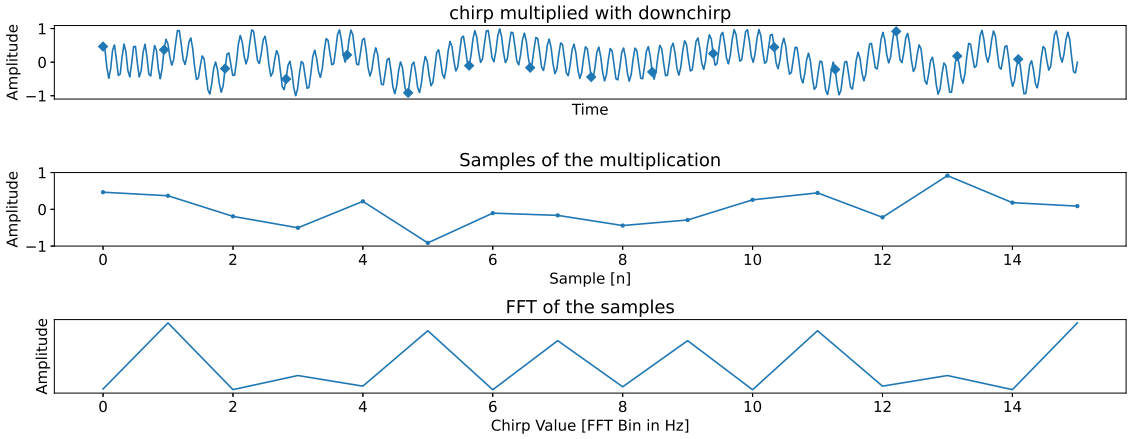

Figure 6.14: **Dechirp process method 3**

6.7.4 Theory

To explain and confirm whether the simplified method 2 can be used and why method 3 cannot, the maths from Chapter 3 are verified for these methods. The equation for a complex chirp is once more provided in Eq. 6.1 but slightly simplified. Using Euler equations, the real component of a complex waveform can be obtained as is shown in Eq. 6.2. To obtain only the real part of the transmitted waveform, the transformation shown in Eq. 6.2 is also applied to Eq. 6.1.

$$c(nT_s + kT) = \underbrace{(e^{j2\pi 2^{SF} k^2 T \frac{B}{2^{SF}}})}_{\text{base up chirp}} \quad \underbrace{(e^{j2\pi[s(nT_s)]kT\frac{B}{2^{SF}}})}_{\text{a pure wave at frequency } s(nT_s)} \tag{6.1}$$

$$y = cos(x) + isin(x) = e^{ix} \rightarrow Re(y) = cos(x) = \frac{e^{ix}}{2i} + \frac{e^{-ix}}{2i} \tag{6.2}$$

For method 2, the real part of Eq. 6.1 is multiplied with the (complex) base-down-chirp from Eq. 3.14. This yields the equation presented in Eq. 6.3 which has three parts, parts A, B and C.
The first component, component A, is a pure wave at frequency $s(nT_s)$. The second component, component B is the base-down-chirp with the frequencies multiplied by a factor of two. The last component, component C, is the complex conjugate of the pure wave at frequency $s(nT_s)$.
The Fourier Transform (FT) will have a high-valued output for the frequency of component A, the pure

wave at frequency $s(nT_s)$. The FT will also have peaks on the frequency response at the other frequencies due to component B and component C, but these are smaller compared to the amplitude at frequency $s(nT_s)$ since they are spread out over the frequency spectrum. For this reason, the true symbol value can be obtained from the chirp signal.

$$d(nT_s + kT) = \frac{\underbrace{(e^{j2\pi[s(nT_s)]kT\frac{B}{2^{SF}}})}_{\text{A}} + (\underbrace{(e^{2(-j\pi 2^{SF}k^2T\frac{B}{2^{SF}})}}_{\text{B}} \times \underbrace{(e^{-j2\pi[s(nT_s)]kT\frac{B}{2^{SF}}})}_{\text{C}})}{2i} \tag{6.3}$$

For method 3, only the real components of both the base down chirp and received chirp are multiplied by each other. The resulting equation now has four components, components D, E, F and G, given in Eq. 6.4. Components D and E are pure waveforms at frequency $s(nT_s)$ but E is D's complex conjugate. This would lead to two equally sized peaks on the FT. From this, the intended symbol value cannot be obtained from dechirping the received chirp. This method could still be used by using only half of the available bits. For example, when an Spreading Factor (SF) of 4 is used, the symbol could have a value from 0 to 15. When transmitting a chirp with symbol value 7 in this example, the bins 7 and 9 will be equally high from the FT. When sending a 5, the bins from the FT will be highest and equally high at 5 and 11. That means that, if you were to transmit only symbol values with a value from 0 to 7, the second half (8 to 15) could be discarded and the symbol can still be decoded by looking at either the bins between 0 and 7 or 8 and 15. Whether checking two peaks rather than one features an extra redundancy was not evaluated. It was found in simulations that this method works best for spreading factors greater than 4.

$$\begin{aligned} d(nT_s + kT) = {} & \underbrace{(e^{j2\pi[s(nT_s)]kT\frac{B}{2^{SF}}})}_{\text{D}} + \\ & \underbrace{(e^{-j2\pi[s(nT_s)]kT\frac{B}{2^{SF}}})}_{\text{E}} + \\ & \underbrace{((e^{2(-j\pi 2^{SF}k^2T\frac{B}{2^{SF}})} \times (e^{-j2\pi[s(nT_s)]kT\frac{B}{2^{SF}}}))}_{\text{F}} + \\ & \underbrace{((e^{-2(-j\pi 2^{SF}k^2T\frac{B}{2^{SF}})} \times (e^{j2\pi[s(nT_s)]kT\frac{B}{2^{SF}}}))}_{\text{G}} \end{aligned} \tag{6.4}$$

Concluding, method 2 can be used to save resources on hardware. For the same spreading factor, the resilience to noise is smaller. When more resources are available due to not using the Hilbert transform, however, increasing the Spreading Factor to overcome the noise resilience, does not require many extra resources but has still a negative effect on the data rate.
Method 3 makes the multiplication more power efficient since only real components have to be multiplied. The downside of this method is that only half of the symbol values for the selected SF can be used.

6.8 Conclusion

This thesis proposed the use of (Frequency Shift) Chirp Spread Spectrum Modulation (FSCSSM) in Body Coupled Communication (BCC) and the impact of varying parameters on its performance was evaluated. Also, the maximum data rate and lowest error-less Signal-to-Noise Ratio (SNR) were assessed. The evaluated parameters were transmitter gain, body composition, Receiver (Rx) and Transmitter (Tx) distance, electrode dimensions, electrode inter-distances, receiver gain, frequency, bandwidth, spreading factor, and noise levels. The evaluations provided insights into the behaviour of the BCC-FSCSSM system under different conditions.

As was already known, centre frequency has no direct influence on data rate, but evaluations revealed that higher centre frequencies had better propagation and allowed for lower SNR. While the centre frequency does not directly improve the data rate, the bandwidth does.

The electrode dimensions- and electrode inter-distance evaluations showed that larger inter-distances might not improve the received signal. From the evaluations, the best inter-distance is suggested to be valued between 1 and 2cm. However, it can be concluded that the inter-distance measurements are hard to perform and not solid. They are not in line with related work. The electrode dimensions do provide a clear result in which smaller electrode dimensions provide less received signal strength in comparison with larger electrode dimensions. The best SNR (lowest) was achieved with the largest electrode dimensions.

In the transmission distance and body composition evaluations it was found that, for single-body communication, the body composition is the leading factor while the distance between Tx and Rx is less important. Especially for low frequencies, the propagation path makes use of muscle tissue and is highly affected by the amount of muscle present. Body-to-body communication was evaluated as well, for the most remote arm of one body to the most remote arm of another body, communication was possible without error.

Noise levels were evaluated by varying SNR, demonstrating the robustness of the BCC-FSCSSM system in handling noise. Triple modular redundancy was shown to improve communication reliability, even in low SNR conditions.

The mathematics of FSCSSM, in Chapter 3, do function but might be simplified by making a trade-off between noise resilience, the use of resources & lack of data rate for increasing the spreading factor and the use of resources for a Hilbert transform. The simplification would be to not obtain the analytical signal from the received signal. One method to not having to make these trade-offs would be sampling both In-Phase and Quadrature signals which might require additional hardware.

Chapter 7

Conclusions

The use of (Frequency Shift) Chirp Spread Spectrum Modulation (FSCSSM) in Body Coupled Communication (BCC) using the Galvanic Coupling (GC) coupling method allows communication with highly noisy channels, up to -9dB Signal-to-Noise Ratio (SNR). Evaluations have shown the possibility of body-to-body communication by touch and the relation between frequency, input voltage and received voltage strength is shown. A higher frequency is found to benefit the system but the upper limits found in related work have not been evaluated in this system. The prototype in this evaluation can communicate to devices all over the body and even at every distance on another body without errors as shown in section 6.5. The greatest achievable data rate of this system, which also achieved communication in a theoretical SNR of -9dB, was 2.4 kilo-symbols per second, in which one symbol is 4 bits, having a total data rate of 9.6 kbps. This improves [48] & [53] and matches [7] of which the first and last use centre frequencies of 8MHz and higher, which was not in the ideal region according to [22]. In terms of noise, all related works have been improved for which none operates beneath the noise floor of 0dB SNR. The finding that, for the low frequencies used in this system, body composition is more important than distance, was not yet stated in related works.

Concluding, this thesis provides valuable insights into the performance and considerations for designing BCC-FSCSSM systems. The results contribute to the understanding of key parameters influencing the system's reliability and pave the way for further advancements in BCC technologies.

With that, the research questions have been asked and with their answers, a prototype was composed that allowed the answering of the main research question as follows:

How does (Frequency Shift) Chirp-Spread-Spectrum Modulation contribute to the performance improvement of Body Coupled Communication with the use of the Galvanic Coupling method while keeping in mind the original intention of body coupled communication?
By using low frequencies, the signal can be coupled into the human body and with the use of FSCSSM, signals with very low signal strength can be transmitted through a highly noisy channel up to a total SNR of -9dB whilst achieving 9.6 kbps data rate.

Chapter 8

Future Work

The prototype in this thesis shows what Body Coupled Communication (BCC) can achieve using (Frequency Shift) Chirp Spread Spectrum Modulation (FSCSSM) with Galvanic Coupling (GC) as a coupling method, but does so only on a prototype scale. The frequencies used are not in the ideal range according to related work and, while the privacy aspect is important for BCC, signal leakage was not evaluated.

It is recommended that research is conducted in which the prototype of this work is implemented in the frequency range found most suitable for GC which is between 1.5 and 2 MHz (on a single body) or between 2 and 4 MHz (on body-to-body communication)[22].

Some research did look into leakage, as was shown in Chapter 2.3 and using their conclusions, the frequencies suggested above and the frequencies used in this thesis are far below the frequency values that lead to leakage. However, this thesis' prototype implements FSCSSM which is intended to be very robust and is used in long-range applications. Because of those two facts, it is suggested for future work to measure the actual reception of the signal outside of the intended body channel. If needed, new limitations for frequencies and input power could be set for GC with FSCSSM from that research.

Arai et al. had different electrode orientations in their work. They placed the electrodes in series with respect to the direction of propagation of the chirp signal. This work placed the electrodes in parallel. The comparison between the two orientation was not evaluated. Such an evaluation is suggested to be performed.

As was found in Chapter 6.7, there might be a possibility to use more simplified maths and that might reduce the number of resources in the receiver. As a future work, it is suggested to evaluate performance differences between using the analytical signal for dechirping and using the real-valued signal for dechirping.
In the related work, Chapter 2.6, a reference to [20] is provided about matching the preamble in LoRa. When using only the real-valued signal, there is no longer the need for sampling according to the Nyquist Sampling Theorem and only 2^{SF} samples have to be taken. Doing so, less positive false flags of finding the preamble will arise and a preamble existing out of a repetition of chirps with symbol values can be implemented. Verification of whether such a preamble gives more redundancy is suggested. More redundancy could increase the symbol success rate.

LoRa PHY has implemented FSCSSM on a physical chip, of which the details are closed-source. Closed source it may be, its operation is validated and for that reason, a simple method for using FSCSSM in BCC might be down-mixing the output of a LoRa chip to the frequencies desired. In the receiver, these could be up-mixed again for another chip to receive and decode the data. With such an implementation a micro-controller can be connected and used to communicate. It is suggested to test this method. If this method were to work, it would become more accessible for development.

Lastly, other modulation schemes have not been tested on this prototype so the evaluation of this

prototype can only be compared to other research. Comparing the performance of FSCSSM with other modulation schemes in the same environment and experimental setup would provide more detailed insights and is thus suggested as future work.

Bibliography

[1] Doaa Ahmed, Jens Kirchner, and Georg Fischer. Signal Transmission with Intra-Body and Inter-Body Communications: Simulation-Based Models. In Chika Sugimoto, Hamed Farhadi, and Matti Hämäläinen, editors, *13th EAI International Conference on Body Area Networks*, EAI/Springer Innovations in Communication and Computing, pages 171–184, Cham, 2020. Springer International Publishing.

[2] Naruto Arai, Dairoku Muramatsu, and Ken Sasaki. Transmission model of Human Body Communication incorporating size and distance between the two electrodes of a transmitter. In *2016 International Conference on Electronics Packaging (ICEP)*, pages 461–464, April 2016.

[3] M. Amparo Callejón, David Naranjo-Hernandez, Javier Reina-Tosina, and Laura M. Roa. Distributed Circuit Modeling of Galvanic and Capacitive Coupling for Intrabody Communication. *IEEE Transactions on Biomedical Engineering*, 59(11):3263–3269, November 2012. Conference Name: IEEE Transactions on Biomedical Engineering.

[4] Maria Amparo Callejón, David Naranjo-Hernández, Javier Reina-Tosina, and Laura M. Roa. A Comprehensive Study Into Intrabody Communication Measurements. *IEEE Transactions on Instrumentation and Measurement*, 62(9):2446–2455, September 2013. Conference Name: IEEE Transactions on Instrumentation and Measurement.

[5] Namjun Cho, Long Yan, Joonsung Bae, and Hoi-Jun Yoo. A 60 kb/s–10 Mb/s Adaptive Frequency Hopping Transceiver for Interference-Resilient Body Channel Communication. *IEEE Journal of Solid-State Circuits*, 44(3):708–717, March 2009. Conference Name: IEEE Journal of Solid-State Circuits.

[6] Debayan Das, Shovan Maity, Baibhab Chatterjee, and Shreyas Sen. Enabling Covert Body Area Network using Electro-Quasistatic Human Body Communication. *Scientific Reports*, 9(1):4160, March 2019. Number: 1 Publisher: Nature Publishing Group.

[7] Taku Hachisu, Baptiste Bourreau, and Kenji Suzuki. EnhancedTouchX: Smart Bracelets for Augmenting Interpersonal Touch Interactions. In *Proceedings of the 2019 CHI Conference on Human Factors in Computing Systems*, CHI '19, pages 1–12, New York, NY, USA, May 2019. Association for Computing Machinery.

[8] Taku Hachisu and Kenji Suzuki. Interpersonal Touch Sensing Devices Using Inter-Body Area Network. *IEEE Sensors Journal*, 21(24):28001–28008, December 2021. Conference Name: IEEE Sensors Journal.

[9] K. Hachisuka, A. Nakata, T. Takeda, Y. Terauchi, K. Shiba, K. Sasaki, H. Hosaka, and K. Itao. Development and performance analysis of an intra-body communication device. In *TRANSDUCERS '03. 12th International Conference on Solid-State Sensors, Actuators and Microsystems. Digest of Technical Papers (Cat. No.03TH8664)*, volume 2, pages 1722–1725 vol.2, June 2003.

[10] K. Hachisuka, Y. Terauchi, Y. Kishi, T. Hirota, K. Sasaki, H. Hosaka, and K. Ito. Simplified circuit modeling and fabrication of intrabody communication devices. In *The 13th International Conference on Solid-State Sensors, Actuators and Microsystems, 2005. Digest of Technical Papers. TRANSDUCERS '05.*, volume 1, pages 461–464 Vol. 1, June 2005. ISSN: 2164-1641.

[11] Nozomi Haga, Kazuyuki Saito, Masaharu Takahashi, and Koichi Ito. Equivalent Circuit of Intrabody Communication Channels Inducing Conduction Currents Inside the Human Body. *IEEE Transactions on Antennas and Propagation*, 61(5):2807–2816, May 2013. Conference Name: IEEE Transactions on Antennas and Propagation.

[12] T. Handa, S. Shoji, S. Ike, S. Takeda, and T. Sekiguchi. A very low-power consumption wireless ECG monitoring system using body as a signal transmission medium. In *Proceedings of International Solid State Sensors and Actuators Conference (Transducers '97)*, volume 2, pages 1003–1006, Chicago, IL, USA, 1997. IEEE.

[13] Prakash Harikumar, Muhammad Irfan Kazim, and J Jacob Wikner. An analog receiver front-end for capacitive body-coupled communication. In *NORCHIP 2012*, pages 1–4, November 2012.

[14] Yongtao Hou, Yong Song, Maoyuan Li, Xu Zhang, Ning Li, Wangwang Zhu, and Yongjia Wang. Design of Image Transmission System of Intra-Body Communication Based on Capacitive Coupling. In *2019 IEEE International Conference on Signal, Information and Data Processing (ICSIDP)*, pages 1–4, December 2019.

[15] ICNIRP. Guidelines for Limiting Exposure to Electromagnetic Fields (100 kHz to 300 GHz). *Health Physics*, 118(5):483–524, May 2020.

[16] IEEE. IEEE Standard for Safety Levels with Respect to Human Exposure to Electric, Magnetic, and Electromagnetic Fields, 0 Hz to 300 GHz. *IEEE Std C95.1-2019 (Revision of IEEE Std C95.1-2005/ Incorporates IEEE Std C95.1-2019/Cor 1-2019)*, pages 1–312, October 2019. Conference Name: IEEE Std C95.1-2019 (Revision of IEEE Std C95.1-2005/ Incorporates IEEE Std C95.1-2019/Cor 1-2019).

[17] Yeseul Jeon, Chongsoo Jung, Song-I Cheon, Hyungjoo Cho, Ji-Hoon Suh, Hyuntak Jeon, Seok-Tae Koh, and Minkyu Je. A 100Mb/s Galvanically-Coupled Body-Channel-Communication Transceiver with 4.75pJ/b TX and 26.8 pJ/b RX for Bionic Arms. In *2019 Symposium on VLSI Circuits*, pages C292–C293, June 2019. ISSN: 2158-5636.

[18] Behailu Kibret, MirHojjat Seyedi, Daniel T. H. Lai, and Micheal Faulkner. Investigation of Galvanic-Coupled Intrabody Communication Using the Human Body Circuit Model. *IEEE Journal of Biomedical and Health Informatics*, 18(4):1196–1206, July 2014. Conference Name: IEEE Journal of Biomedical and Health Informatics.

[19] Behailu Kibret, Assefa K. Teshome, and Daniel T. H. Lai. HUMAN BODY AS ANTENNA AND ITS EFFECT ON HUMAN BODY COMMUNICATIONS. *Progress In Electromagnetics Research*, 148:193–207, 2014.

[20] M. Knight and B. Seeber. Decoding LoRa: Realizing a Modern LPWAN with SDR. In *Proceedings of the GNU Radio Conference*, volume 1 of *1*, September 2016.

[21] Hongqiang Li, Yubing Zhang, Xu Zhao, and Xiaoke Tang. Demodulation of Frequency Shift Chirp Spreading spectrum with Cyclic Prefix. In *2020 15th IEEE International Conference on Signal Processing (ICSP)*, volume 1, pages 433–438, December 2020. ISSN: 2164-5221.

[22] Maoyuan Li, Yong Song, Wansong Li, Guangfa Wang, Tianpeng Bu, Yufei Zhao, and Qun Hao. The Modeling and Simulation of the Galvanic Coupling Intra-Body Communication via Handshake Channel. *Sensors (Basel, Switzerland)*, 17, April 2017.

[23] Shovan Maity, Debayan Das, Xinyi Jiang, and Shreyas Sen. Secure Human-Internet using dynamic Human Body Communication. In *2017 IEEE/ACM International Symposium on Low Power Electronics and Design (ISLPED)*, pages 1–6, July 2017.

[24] Shovan Maity, Mingxuan He, Mayukh Nath, Debayan Das, Baibhab Chatterjee, and Shreyas Sen. Bio-Physical Modeling, Characterization, and Optimization of Electro-Quasistatic Human Body Communication. *IEEE Transactions on Biomedical Engineering*, 66(6):1791–1802, June 2019. Conference Name: IEEE Transactions on Biomedical Engineering.

[25] Shovan Maity, David Yang, Scott Stanton Redford, Debayan Das, Baibhab Chatterjee, and Shreyas Sen. BodyWire-HCI: Enabling New Interaction Modalities by Communicating Strictly During Touch Using Electro-Quasistatic Human Body Communication. *ACM Transactions on Computer-Human Interaction*, 27(6):39:1–39:25, November 2020.

[26] Nirmoy Modak, Mayukh Nath, Baibhab Chatterjee, Shovan Maity, and Shreyas Sen. Bio-Physical Modeling of Galvanic Human Body Communication in Electro-Quasistatic Regime. *IEEE Transactions on Biomedical Engineering*, 69(12):3717–3727, December 2022. Conference Name: IEEE Transactions on Biomedical Engineering.

[27] Dairoku Muramatsu and Ken Sasaki. LED Control System Using Human Body Communication Between Two Users. In *Proceedings of the 2018 ACM International Joint Conference and 2018 International Symposium on Pervasive and Ubiquitous Computing and Wearable Computers*, UbiComp '18, pages 408–411, New York, NY, USA, October 2018. Association for Computing Machinery.

[28] Dairoku Muramatsu and Ken Sasaki. Signal propagation analysis in multiuser human body communication. In *Adjunct Proceedings of the 2019 ACM International Joint Conference on Pervasive and Ubiquitous Computing and Proceedings of the 2019 ACM International Symposium on Wearable Computers*, UbiComp/ISWC '19 Adjunct, pages 157–159, New York, NY, USA, September 2019. Association for Computing Machinery.

[29] Mayukh Nath, Shovan Maity, Shitij Avlani, Scott Weigand, and Shreyas Sen. Inter-body coupling in electro-quasistatic human body communication: theory and analysis of security and interference properties. *Scientific Reports*, 11(1):4378, February 2021.

[30] Yoshifumi Nishida, Ken Sasaki, Kentaro Yamamoto, Dairoku Muramatsu, and Fukuro Koshiji. Equivalent Circuit Model Viewed From Receiver Side in Human Body Communication. *IEEE Transactions on Biomedical Circuits and Systems*, 13(4):746–755, August 2019. Conference Name: IEEE Transactions on Biomedical Circuits and Systems.

[31] Jiwoong Park, Harinath Garudadri, and Patrick P. Mercier. Channel Modeling of Miniaturized Battery-Powered Capacitive Human Body Communication Systems. *IEEE Transactions on Biomedical Engineering*, 64(2):452–462, February 2017. Conference Name: IEEE Transactions on Biomedical Engineering.

[32] Jiwoong Park and Patrick P. Mercier. Magnetic human body communication. In *2015 37th Annual International Conference of the IEEE Engineering in Medicine and Biology Society (EMBC)*, pages 1841–1844, August 2015. ISSN: 1558-4615.

[33] Gianni Pasolini. On the LoRa Chirp Spread Spectrum Modulation: Signal Properties and Their Impact on Transmitter and Receiver Architectures. *IEEE Transactions on Wireless Communications*, 21(1):357–369, January 2022. Conference Name: IEEE Transactions on Wireless Communications.

[34] M Pavithra and U Udayanila. Red Tacton Technology. *International Journal of Engineering Research*, 3(15), 2015.

[35] Maicon D. Pereira, Germán A. Alvarez-Botero, and Fernando Rangel de Sousa. Characterization and Modeling of the Capacitive HBC Channel. *IEEE Transactions on Instrumentation and Measurement*, 64(10):2626–2635, October 2015. Conference Name: IEEE Transactions on Instrumentation and Measurement.

[36] Ian Sample and Ian Sample Science editor. Paralysed man walks using device that reconnects brain with muscles. *The Guardian*, May 2023.

[37] A. Sasaki, M. Shinagawa, and K. Ochiai. Sensitive and stable electro-optic sensor for intrabody communication. In *The 17th Annual Meeting of the IEEELasers and Electro-Optics Society, 2004. LEOS 2004.*, volume 1, pages 122–123 Vol.1, November 2004.

[38] Ai-ichiro Sasaki, Mitsuru Shinagawa, and Katsuyuki Ochiai. Principles and Demonstration of Intrabody Communication With a Sensitive Electrooptic Sensor. *IEEE Transactions on Instrumentation and Measurement*, 58(2):457–466, February 2009. Conference Name: IEEE Transactions on Instrumentation and Measurement.

[39] Ken Sasaki, Dairoku Muramatsu, Naruto Arai, and Fukuro Koshiji. Evaluation of ground loop through the floor in human body communication. In *2016 10th International Symposium on Medical Information and Communication Technology (ISMICT)*, pages 1–2, March 2016. ISSN: 2326-8301.

[40] Shreyas Sen. SocialHBC: Social Networking and Secure Authentication using Interference-Robust Human Body Communication. In *Proceedings of the 2016 International Symposium on Low Power Electronics and Design*, ISLPED '16, pages 34–39, New York, NY, USA, August 2016. Association for Computing Machinery.

[41] MirHojjat Seyedi, Behailu Kibret, Daniel T. H. Lai, and Michael Faulkner. A Survey on Intrabody Communications for Body Area Network Applications. *IEEE Transactions on Biomedical Engineering*, 60(8):2067–2079, August 2013. Conference Name: IEEE Transactions on Biomedical Engineering.

[42] M. Shinagawa, M. Fukumoto, K. Ochiai, and H. Kyuragi. A near-field-sensing transceiver for intrabody communication based on the electrooptic effect. *IEEE Transactions on Instrumentation and Measurement*, 53(6):1533–1538, December 2004. Conference Name: IEEE Transactions on Instrumentation and Measurement.

[43] Mariam Sunny and Pooja Desai. Musk's Neuralink to start human trial of brain implant for paralysis patients. *Reuters*, September 2023.

[44] Kenji Suzuki, Taku Hachisu, and Kazuki Iida. EnhancedTouch: A Smart Bracelet for Enhancing Human-Human Physical Touch. In *Proceedings of the 2016 CHI Conference on Human Factors in Computing Systems*, CHI '16, pages 1282–1293, New York, NY, USA, May 2016. Association for Computing Machinery.

[45] William J. Tomlinson, Stella Banou, Shay Blechinger-Slocum, Christopher Yu, and Kaushik R. Chowdhury. Body-Guided Galvanic Coupling Communication for Secure Biometric Data. *IEEE Transactions on Wireless Communications*, 18(8):4143–4156, August 2019. Conference Name: IEEE Transactions on Wireless Communications.

[46] William J. Tomlinson, Stella Banou, Christopher Yu, Milica Stojanovic, and Kaushik R. Chowdhury. Comprehensive Survey of Galvanic Coupling and Alternative Intra-Body Communication Technologies. *IEEE Communications Surveys & Tutorials*, 21(2):1145–1164, 2019. Conference Name: IEEE Communications Surveys & Tutorials.

[47] Lorenzo Vangelista. Frequency Shift Chirp Modulation: The LoRa Modulation. *IEEE Signal Processing Letters*, 24(12):1818–1821, December 2017. Conference Name: IEEE Signal Processing Letters.

[48] Virag Varga, Marc Wyss, Gergely Vakulya, Alanson Sample, and Thomas R. Gross. Designing Groundless Body Channel Communication Systems: Performance and Implications. In *Proceedings of the 31st Annual ACM Symposium on User Interface Software and Technology*, UIST '18, pages 683–695, New York, NY, USA, October 2018. Association for Computing Machinery.

[49] Hao Wang, Xian Tang, Chiu Sing Choy, and Gerald E. Sobelman. Cascaded Network Body Channel Model for Intrabody Communication. *IEEE Journal of Biomedical and Health Informatics*, 20(4):1044–1052, July 2016. Conference Name: IEEE Journal of Biomedical and Health Informatics.

[50] Meng Wang, ZeTian Wang, JiaWen Li, and Feng Wan. Architectural hardware design of modulator and demodulator for galvanic coupling intra-body communication. In *The 7th 2014 Biomedical Engineering International Conference*, pages 1–4, November 2014.

[51] Marc Wegmueller, Adrian Lehner, Juerg Froehlich, Robert Reutemann, Michael Oberle, Norbert Felber, Niels Kuster, Otto Hess, and Wolfgang Fichtner. Measurement System for the Characterization of the Human Body as a Communication Channel at Low Frequency. In *2005 IEEE Engineering in Medicine and Biology 27th Annual Conference*, pages 3502–3505, Shanghai, 2005. IEEE.

[52] Marc Simon Wegmueller, Michael Oberle, Norbert Felber, Niels Kuster, and Wolfgang Fichtner. Signal Transmission by Galvanic Coupling Through the Human Body. *IEEE Transactions on Instrumentation and Measurement*, 59(4):963–969, April 2010. Conference Name: IEEE Transactions on Instrumentation and Measurement.

[53] He Jing Wu, Yue-Ming Gao, Sio Hang Pun, Peng Un Mak, and Mang I. Vai. A Transceiver Designed For Intra-body Communication of Body Area Networks. In *6th International ICST Conference on Body Area Networks*, June 2012.

[54] Zhenqiang Xu, Shuai Tong, Pengjin Xie, and Jiliang Wang. From Demodulation to Decoding: Toward Complete LoRa PHY Understanding and Implementation. *ACM Transactions on Sensor Networks*, 18(4):64:1–64:27, January 2023.

[55] Kentaro Yamamoto, Yoshifumi Nishida, Ken Sasaki, Dairoku Muramatsu, and Fukuro Koshiji. Electromagnetic Field Analysis of Signal Transmission Path and Electrode Contact Conditions in Human Body Communication. *Applied Sciences*, 8(9):1539, September 2018. Number: 9 Publisher: Multidisciplinary Digital Publishing Institute.

[56] David Yang, Shovan Maity, and Shreyas Sen. Physically Secure Wearable–Wearable Through-Body Interhuman Body Communication. *Frontiers in Electronics*, 2, 2022.

[57] David Yang, Parikha Mehrotra, Scott Weigand, and Shreyas Sen. In-the-Wild Interference Characterization and Modelling for Electro-Quasistatic-HBC With Miniaturized Wearables. *IEEE Transactions on Biomedical Engineering*, 68(9):2858–2869, September 2021. Conference Name: IEEE Transactions on Biomedical Engineering.

[58] Xu Zhang, Yong Song, Wu Ren, Yufei Zhao, Yu Chen, Wangwang Zhu, Dongliang Zhou, and Changxiang Li. Model and channel characteristics of near field inter-body coupling communication. *AEU - International Journal of Electronics and Communications*, 156:154385, November 2022.

[59] Jian Feng Zhao, Xi Mei Chen, Bo Dong Liang, and Qiu Xia Chen. A Review on Human Body Communication: Signal Propagation Model, Communication Performance, and Experimental Issues. *Wireless Communications and Mobile Computing*, 2017:1–15, October 2017.

[60] T. G. Zimmerman. Personal area networks: Near-field intrabody communication. *IBM Systems Journal*, 35(3,4):609–617, 1996. Num Pages: 9 Place: Armonk, United States Publisher: International Business Machines Corporation.

Appendix A

Oscilloscope measurements

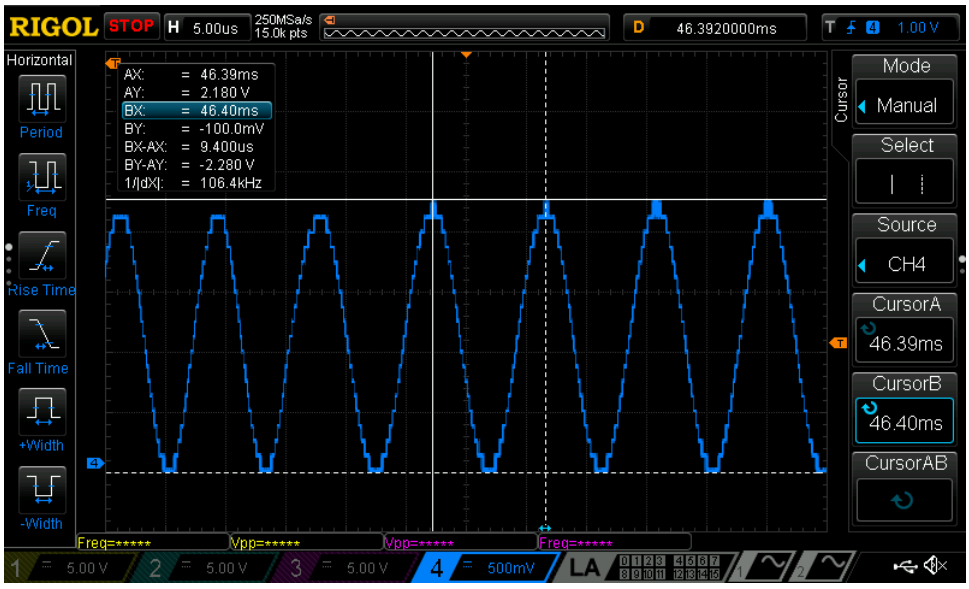

Figure A.1: **Input voltage of a chirp measured across the transmitter electrodes on the body**

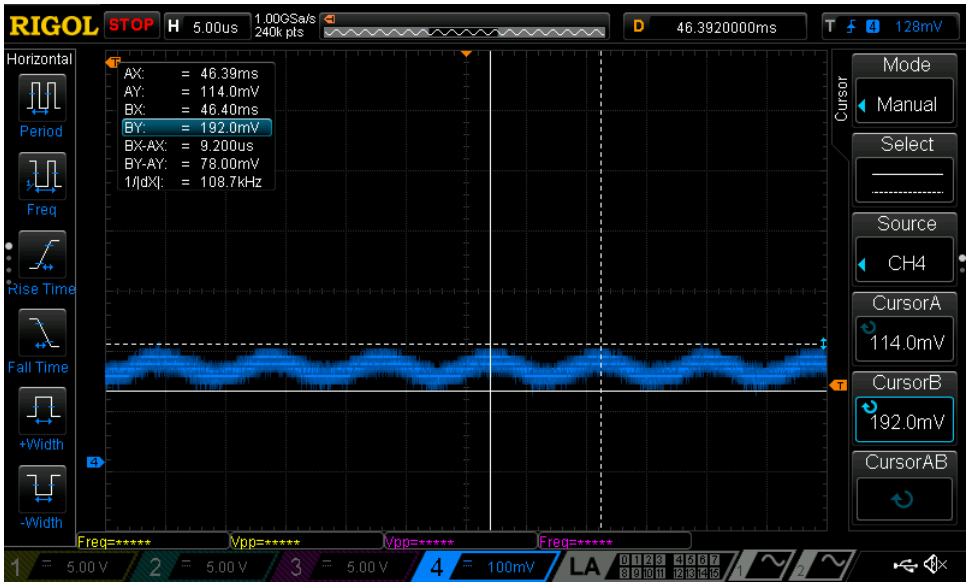

Figure A.2: **Out voltage of a chirp measured across the receiver electrodes on the body**

Appendix B

Electrical schematics

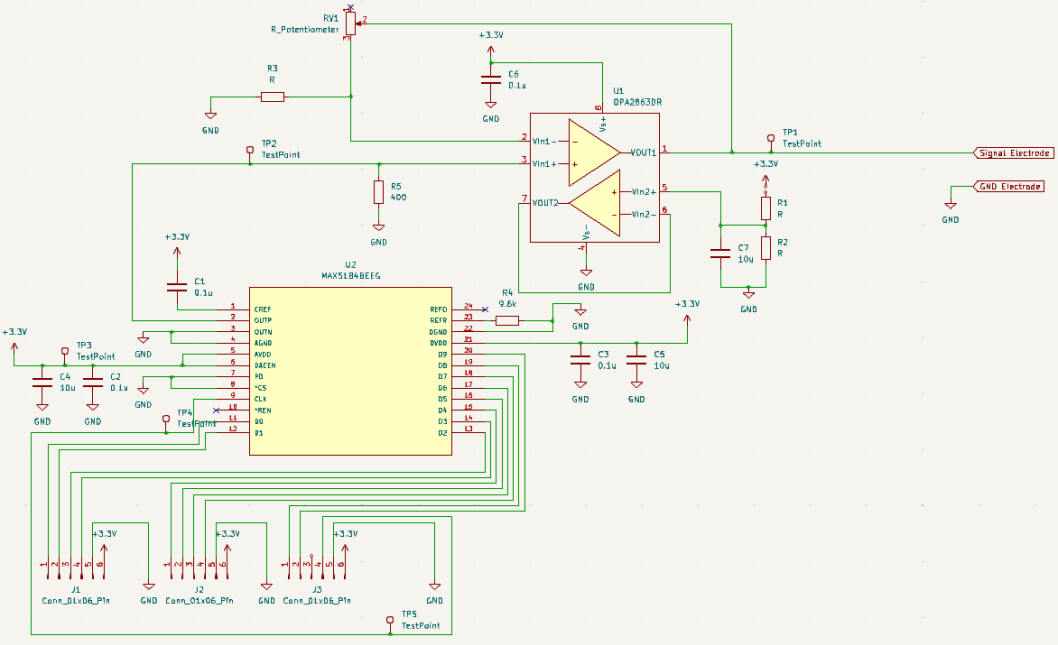

Figure B.1: **Schematic of the transmitter circuit used in this thesis.**

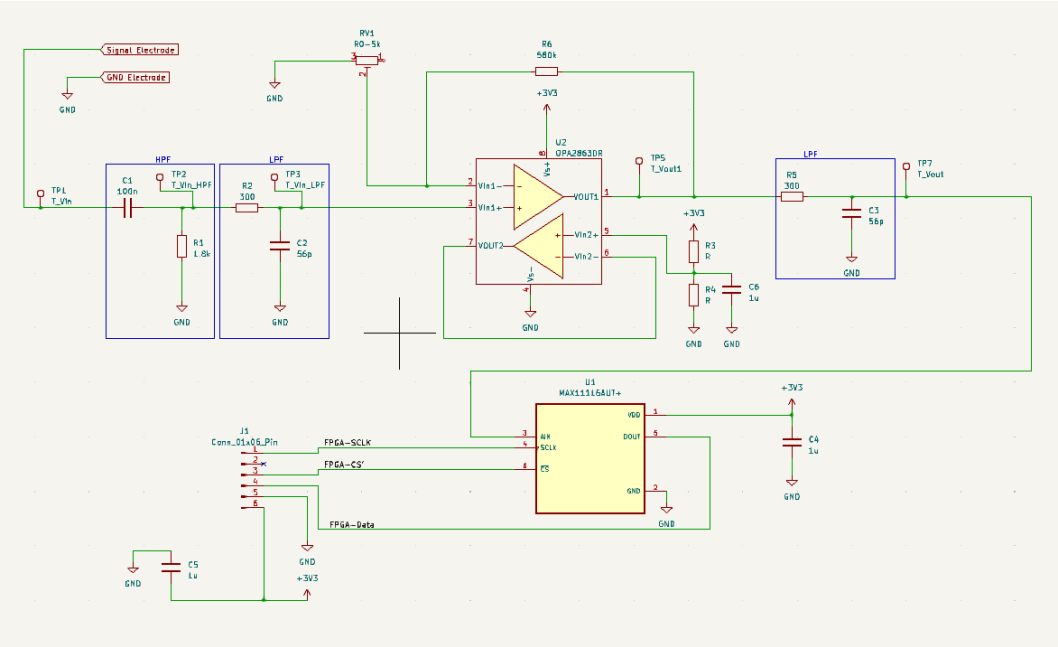

Figure B.2: **Schematic of the receiver circuit used in this thesis.**

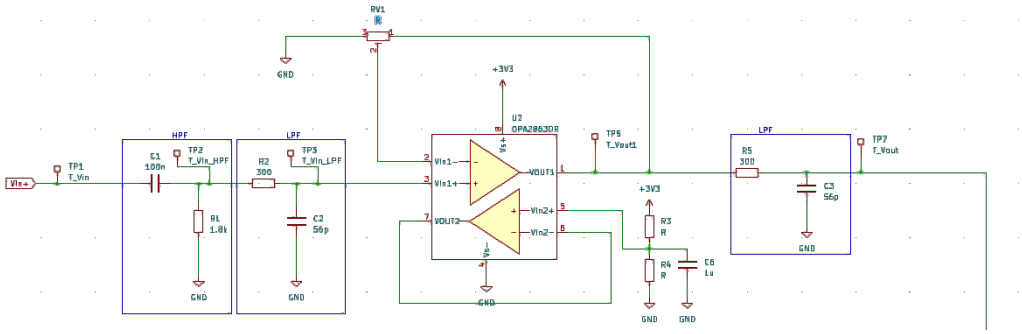

Figure B.3: **Example schematic for an analog-front-end that can be used on the Body Coupled Communication (BCC) receiver.**